Research Square

Preprints are preliminary reports that have not undergone peer review.
They should not be considered conclusive, used to inform clinical practice,
or referenced by the media as validated information.

Localized patterns and their moving dynamics in a diffusive population-toxicant model with negative toxicant-taxis

Zhenzhen Li
Central South University
Zhian Wang
Hong Kong Polytechnic University
Shuangquan Xie
xieshuangquan@hnu.edu.cn
Hunan University
Haidong Yang
Central South University

Research Article

Keywords:

Posted Date: November 2nd, 2026

DOI: https://doi.org/10.21203/rs.3.rs-10973195/v1

License: This work is licensed under a Creative Commons Attribution 4.0 International License.
Read Full License

Additional Declarations: No competing interests reported.

Localized patterns and their moving dynamics in a diffusive population-toxicant model with negative toxicant-taxis

Zhenzhen Li*, Zhi-An Wang†, Shuangquan Xie‡ and Haidong Yang§

September 8, 2026

Abstract. We investigate the existence of aggregation patterns and their moving dynamics in the population-toxicant model proposed in [10], which incorporates the spatial avoidance response of a population to toxicants characterized by a negative (repulsive) toxicant-taxis term. In the limit of large toxicant-taxis sensitivity, we explicitly construct asymptotic equilibrium spike solutions using formal matched asymptotic expansions, and show that boundary spikes are linearly stable at leading order. In contrast, by deriving an explicit asymptotic formula for the translational eigenvalue, we show that interior spike solutions are linearly unstable to translations of the spike profile. We further derive a reduced system of ordinary differential equations describing the fast motion of the spike center and the slow motion of the spike height for both spatially homogeneous and inhomogeneous toxicant inputs. Our results reveal that spikes drift rapidly toward the nearest domain boundary in homogeneous environments, while they converge to a stable local minimum of the background toxicant concentration in strongly inhomogeneous environments. These asymptotic findings offer a new research direction for subsequent rigorous analytical work.

Keywords. Population-toxicant model; toxicant-taxis; spike patterns; fast and slow motion

2020 MSC. 92D25, 35K57, 35K55, 35Q92

1 Introduction

Water pollution, caused by the release of hazardous chemical contaminants into lakes, rivers, oceans, and other aquatic ecosystems, remains one of the major global environmental challenges [1, 30, 31]. Toxic substances in aquatic environments can affect organisms at multiple biological levels, ranging from individual physiology and behavior to population persistence and community structure. It is therefore important to understand how toxicants influence population dynamics and to identify the mechanisms that determine whether a population persists or becomes extinct in a polluted habitat.

*School of Mathematics and Statistics, Central South University, Changsha, 410083, P.R. China; email address: zhzhli94@163.com

†Department of Applied Mathematics, The Hong Kong Polytechnic University, Kowloon, Hong Kong; email address: mawza@polyu.edu.hk

‡School of Mathematics, Hunan University, Changsha, 410082, P. R. China; email address: xieshuangquan@hnu.edu.cn

§School of Mathematics and Statistics, Central South University, Changsha, 410083, P.R. China; email address: hdyang@csu.edu.cn.

Over the past four decades, a rich body of mathematical models based on ordinary differential equations (ODEs) has been developed to study population-toxicant interactions in polluted environments [12–16, 25, 34]. These models typically describe the temporal evolution of population biomass, toxicant concentrations in organisms, and toxicant concentrations in the environment. However, ODE models inherently neglect spatial heterogeneity in both population distribution and toxicant concentration, despite the fact that both populations and toxicants spread spatially through active movement and passive diffusion driven by water turbulence.

Furthermore, extensive empirical evidence has documented profound behavioral changes induced by toxicant exposure, including altered habitat preference, impaired predator avoidance, and increased migration [2, 3, 31]. Most notably, individuals often actively flee from areas of high toxicant concentration to regions of lower toxicity to enhance their survival, growth, and reproductive success [38]. To incorporate these spatial and behavioral effects, Deng et al. [10] recently proposed a spatiotemporal model with negative toxicant-taxis that describes the interactions between a population and a toxicant in a closed and contaminated aquatic habitat:

$$\begin{cases} u_t = d_1 u_{xx} + \chi(uw_x)_x + u(r - mw) - au^2, & \text{in } \Omega \\ w_t = d_2 w_{xx} + h(x) - gw - buw, & \text{in } \Omega \\ \partial_\nu u = \partial_\nu w = 0, & \text{on } \partial\Omega \end{cases} \tag{1.1}$$

where $u(x,t)$ denotes the population density and $w(x,t)$ denotes the environmental toxicant concentration. The constants $d_1 > 0$ and $d_2 > 0$ are the diffusion rates of the population and toxicant, respectively; $r > 0$ is the intrinsic growth rate of the population; $m > 0$ measures the harmful effect of the toxicant on population growth; $a > 0$ is the strength of intraspecific competition; $h(x) \geq 0$ is the space-dependent toxicant input; $g > 0$ is the toxicant degradation rate; and $b > 0$ measures the absorption of toxicant due to interaction with the population. ν denotes the outward unit normal vector of $\partial\Omega$ and the homogeneous Neumann conditions indicate that no flux can cross the boundary, relevant to the closed habitat.

Deng et al. [10] first established the global well-posedness of solutions in two dimensions and further studied the effects of toxicants on the spatial pattern formation. They showed that, under suitable low constant input of the toxicant, the population and toxicant may coexist either in a spatially homogeneous state when the taxis sensitivity χ is small, or in a spatially heterogeneous state when χ is large. A central conclusion of their analysis is that random diffusion alone does not destabilize the homogeneous coexistence equilibrium, whereas sufficiently strong toxicant-taxis can do so. This indicates that active avoidance of high-toxicity regions is a key mechanism driving the emergence of spatially inhomogeneous populations and toxicant distributions in a spatially homogeneous environment. However, the detailed structural characteristics of these inhomogeneous patterns remain largely unexplored. Intuitively, populations tend to aggregate in regions with the lowest toxicant concentrations, a phenomenon numerically demonstrated in [10]. Nevertheless, a rigorous mathematical proof for such segregated aggregation behavior is still lacking. As a preliminary attempt to address this open problem, this paper investigates the limiting regime where toxicant-taxis governs the system dynamics, namely $\chi \gg 1$.

Localized aggregation patterns, often called "spikes", have been extensively studied in attractive (or positive) chemotaxis models, especially in Keller-Segel type systems where individuals move towards chemical gradients [11, 19–24, 26, 28, 37]. By contrast, the toxicant-taxis mechanism in (1.1) is repulsive: individuals move away from chemical gradients. Repulsive chemotaxis is often expected to suppress aggregation and stabilize to spatially homogeneous states [6, 17]. It is therefore a little surprising and somewhat counterintuitive that the population-toxicant system considered here can exhibit sharply localized population spikes.

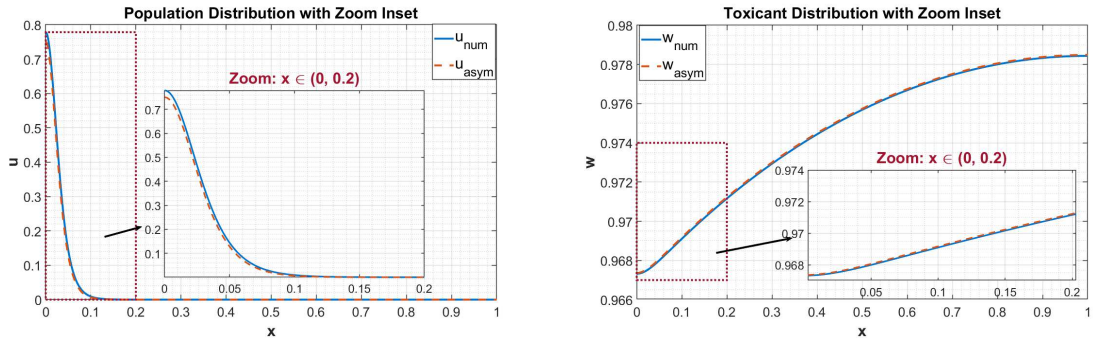


Figure 1: Comparison of the numerical boundary spike (solid blue) with the asymptotic profile (1.3) (dashed red) on the half-domain $0 < x < \ell$. The numerical solution is obtained by solving (1.2) with homogeneous Neumann conditions at $x = 0$ and $x = \ell$ up to $t = 10^5$, starting from $u(x,0) = e^{-50x^2}$ and $w(x,0) = 1$. The parameters are $\varepsilon = 2 \times 10^{-2}$, $\ell = 1$, $D = 1$, $h = 1$, $m = 0.5$, $a = b = \tau = r = 1$. All the numerical simulations are computed using FlexPDE7 [29].

1.1 Main results

In this paper, we analyze system (1.1) in the limit of large toxicant-taxis sensitivity (i.e., $\chi \gg 1$) in one dimension $\Omega = [-\ell, \ell]$. To facilitate the analysis, we introduce the following rescalings:

$$\tilde{t} = d_1 t,\ \varepsilon^2 = \frac{d_1}{\chi},\ D = \frac{d_2}{g},\ \tilde{r} = \frac{r}{d_1},\ \tilde{m} = \frac{m}{d_1},\ \tilde{a} = \frac{a}{d_1},\ \tilde{b} = \frac{b}{g},\ \tilde{h}(x) = \frac{h(x)}{g},\ \tau = \frac{d_1}{g}.$$

Substituting the above rescalings into (1.1) and dropping the tildes for notational simplicity, we obtain the following rescaled system

$$\begin{cases} u_t = u_{xx} + \varepsilon^{-2}(uw_x)_x + u(r - mw) - au^2, & -\ell < x < \ell, \quad t > 0, \\ \tau w_t = Dw_{xx} + h(x) - w - buw, & -\ell < x < \ell, \quad t > 0, \\ u_x(\pm\ell, t) = w_x(\pm\ell, t) = 0, & t > 0. \end{cases} \tag{1.2}$$

Previous studies of population-toxicant systems have addressed global existence of solutions and taxis-induced pattern formation [10], as well as the existence of nonconstant steady states [7,40]. More recent extensions have considered boundary toxicant input [18], delayed toxicant response [32], and time-periodic toxicant input [8]. However, the singular structure, spectral stability, and motion of localized spikes in the large toxicant-taxis limit have not been analyzed. We address these questions below using matched asymptotic expansions.

First, we construct an asymptotic equilibrium boundary spike solution on the half-domain $(0, \ell)$, see Figure 1, using the method of matched asymptotic expansions.

Proposition 1.1. *Suppose the toxicant input rate is constant, $h(x) \equiv h > 0$, and the population growth condition $r - mh > 0$ holds. Then for $0 < \varepsilon \ll 1$, the steady-state problem associated with (1.2) on $(0, \ell)$, subject to the Neumann boundary conditions $u_x(0) = u_x(\ell) = w_x(0) = w_x(\ell) = 0$, formally admits a positive nonconstant boundary-spike profile (u_s, w_s) centered at $x = 0$, which has the asymptotic expansion*

$$\begin{aligned} u_s(x) &\sim \bar{A}\,\mathrm{sech}^2\left(\sqrt{\frac{\bar{A}bh}{2D}}\frac{x}{\varepsilon}\right), \\ w_s(x) &\sim h - \varepsilon s_0 G(x) - \varepsilon^2\left(s_1 G(x) + \ln\left(\mathrm{sech}^2\left(\sqrt{\frac{\bar{A}bh}{2D}}\frac{x}{\varepsilon}\right)\right) + \sqrt{\frac{2\bar{A}bh}{D}}\frac{x}{\varepsilon} - 2\ln 2\right), \end{aligned} \tag{1.3}$$

where $\bar{A} = \frac{3(r-mh)}{2a}$, s_0, s_1 are constants determined by (2.39) and $G(x)$ is the Green's function defined by (2.27) in Section 2. In particular, the leading-order function $\bar{A}\,\mathrm{sech}^2\left(\sqrt{\frac{\bar{A}bh}{2D}}\frac{x}{\varepsilon}\right)$ is strictly decreasing for $x \in (0, \ell)$.

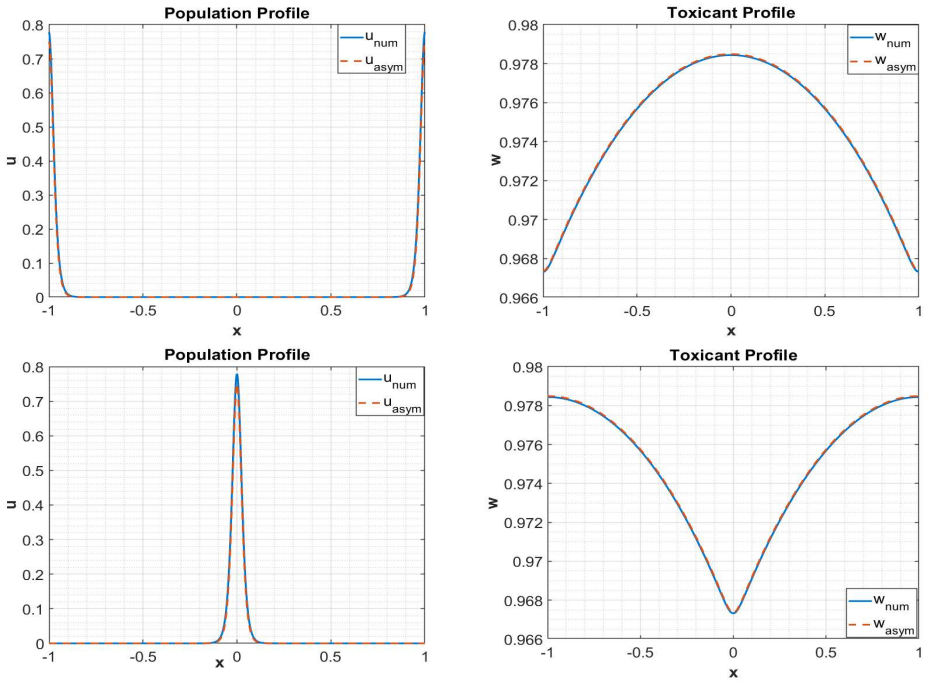


Figure 2: The subfigures at the top (resp. bottom) show that the numerical double boundary spike (resp. single interior spike) $(u_{\rm num}, w_{\rm num})$ marked by a solid blue line agrees well with the double boundary spike (resp. single interior spike) $(u_{\rm asym}, w_{\rm asym})$ marked by a dashed red line given in (1.4) and (1.5) with $\varepsilon = 2.0 \times 10^{-2}$ and interval length $\ell = 1$. The remaining parameters are $D = 1, h = 1, m = 0.5, a = 1, b = 1, \tau = 1, r = 1$. The numerical double boundary spike and single interior spike (solid blue) are obtained by numerically solving the time-dependent system (1.2), similar to those shown in Figure 1 except that the initial conditions are given by $u(x,0) = e^{-50(x+1)^2} + e^{-50(x-1)^2}$, $w(x,0) = 1$ for the double-boundary spike, and $u(x,0) = e^{-50x^2}$, $w(x,0) = 1$ for the single interior spike.

Then, by periodic reflection of the formal half-spike profile, one obtains two classes of formal n-spike asymptotic approximations:

Corollary 1.1. *Let $n \geq 1$ be any fixed integer and $u_s(x;\ell)$, $w_s(x;\ell)$ be the half-spike solution constructed in (1.3) in the interval $(0,\ell)$. Then, as $\varepsilon \to 0^+$, periodic reflection of the half-spike profile defines two classes of formal symmetric n-spike asymptotic approximations:*

- *Double boundary spike patterns:*

$$(\mathbf{u}_n^-, \mathbf{w}_n^-)(x) = (0,h) + (u_s, w_s - h)\left(\min_{0\leq j\leq n}\left|x + \ell - \frac{2j\ell}{n}\right|; \frac{\ell}{n}\right), \quad x \in (-\ell, \ell). \tag{1.4}$$

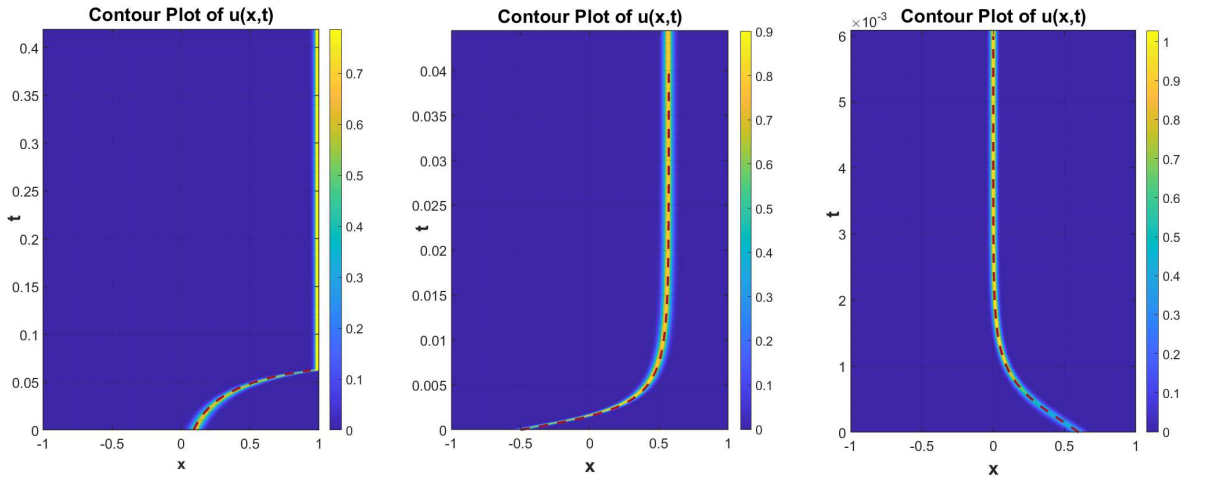
- *Interior spike patterns:*

$$(\mathbf{u}_n^+, \mathbf{w}_n^+)(x) = (0,h) + (u_s, w_s - h)\left(\min_{1\leq j\leq n}\left|x - \ell + \frac{(2j-1)\ell}{n}\right|; \frac{\ell}{n}\right), \quad x \in (-\ell, \ell). \tag{1.5}$$

These expressions are understood as formal leading-order approximations; no rigorous existence assertion is made here. Figure 2 illustrates the double boundary spike pattern and the single interior spike pattern we have constructed. Our asymptotic solution is in good agreement with the numerical solution.

Next, we perform a linear stability analysis of these spike solutions.

Proposition 1.2. *Assume that $r - mh > 0$ and that $\tau \geq 0$ is fixed independently of ε. As $\varepsilon \to 0^+$, the formal stability analysis gives the following conclusions:*



(a) Homogeneous input (b) Weak inhomogeneous input (c) Strong inhomogeneous input.

Figure 3: Drift dynamics of a single interior spike. The color plots show numerical solutions of (1.2), and the dashed red curves show the spike-center trajectories predicted by (1.6) in panels (a) and (b), and by (1.9) in panel (c). The common parameters are $D = a = b = r = \ell = 1$, $m = 0.5$, and $\varepsilon = 2\times 10^{-2}$. In (a), $h(x) = h_0 = 1$, $x_0(0) = 0.1$, and $\tau = \varepsilon^2$. In (b), $h(x) = h_0 + \varepsilon h_1(x)$ with $h_0 = 1$, $\bar{v}_x(x) = -10(1-x^2)(x-0.5)$, $h_1 = D\bar{v}_{xx} - \bar{v}$, $x_0(0) = -0.5$, and $\tau = \varepsilon^2$. For panels (a) and (b), the initial data are $u(x,0) = \bar{A}_0 \mathrm{sech}^2\left(\sqrt{\frac{\bar{A}_0 b h_0}{2D}}\,\frac{x-x_0(0)}{\varepsilon}\right)$, $w(x,0) = h_0$, $\bar{A}_0 = \frac{3(r-mh_0)}{2a}$. In (c), $h(x) = 1 + \left[D\left(\frac{\pi}{\ell}\right)^2 + 1\right]^{-1} - \cos\left(\frac{\pi x}{\ell}\right)$, $x_0(0) = 0.6$, and $\tau = \varepsilon^2$. The corresponding initial data are $u(x,0) = \bar{A}_0 \exp\left[-\frac{(x-x_0(0))^2}{\varepsilon^2}\right]$, $w(x,0) = \bar{w}(x)$, where $\bar{w}$ solves $D\bar{w}_{xx} + h(x) - \bar{w} = 0$ with $\bar{w}_x(\pm\ell) = 0$.

- *The single boundary spike solution constructed in Proposition 1.1 is linearly stable.*
- *The double boundary spike solution* (1.4) *with* $n = 1$ *is linearly stable.*
- *The single interior spike solution* (1.5) *with* $n = 1$ *is linearly unstable due to a positive translational eigenvalue.*

Although the leading inner spike profile is related to the Type I structure studied by Kolokolnikov, Wei and Alcolado [20], the spectral problem obtained here has a different coupled structure. For the boundary spike, we derive a large-core eigenvalue problem and use a coercive energy identity, together with a nonlocal quadratic-form estimate, to exclude all nonzero eigenvalues in the closed right half-plane. For the interior spike, the translational instability exhibits a distinguished τ/ε crossover: its eigenvalue is $\mathcal{O}(1)$ when $\tau > 0$ is fixed, but becomes $\mathcal{O}(\varepsilon^{-1})$ when $\tau = \mathcal{O}(\varepsilon)$, including the instantaneous-response limit $\tau = 0$.

The translational instability of interior spikes induces drift motion of the spike center; see Figure 3 for a contour plot of the spatiotemporal dynamics of an interior spike. To isolate this effect, we consider the limit $\tau \to 0$ where the toxicant evolves instantaneously relative to the population.

Proposition 1.3. *In the limit* $\tau = 0$ *with a weakly spatially varying toxicant input* $h(x) = h_0 + \varepsilon h_1(x)$*, an interior spike initially located at* x_0 *with profile*

$$u(x) \sim \bar{A}\,\mathrm{sech}^2\left(\sqrt{\frac{\bar{A}bh_0}{2D}}\,\frac{x-x_0}{\varepsilon}\right)$$

evolves according to the following ODE system at leading order

$$\frac{dx_0}{dt} = \frac{1}{\varepsilon}\left(\bar{v}_x(x_0) + \sqrt{\frac{2bh_0\bar{A}}{D}}\frac{\tanh\left(\frac{x_0-\ell}{\sqrt{D}}\right)+\tanh\left(\frac{\ell+x_0}{\sqrt{D}}\right)}{\tanh\left(\frac{\ell-x_0}{\sqrt{D}}\right)+\tanh\left(\frac{\ell+x_0}{\sqrt{D}}\right)}\right), \tag{1.6}$$

$$\frac{d\bar{A}}{dt} = 2(r-mh_0)\bar{A} - \frac{4a}{3}\bar{A}^2, \tag{1.7}$$

where $\bar{v}$ is the unique solution to

$$D\bar{v}_{xx} - \bar{v} - h_1(x) = 0, \quad \bar{v}_x(\pm\ell) = 0. \tag{1.8}$$

When spatial inhomogeneity in the toxicant input is strong, the first term in (1.6) dominates the spike drift dynamics. In fact, formal asymptotic analysis shows the leading-order motion of the spike center is universally described by the following simple ODE, independent of the spike's detailed internal structure and subject only to spatial localization of the solution.

Proposition 1.4. *In the instantaneous-response limit $\tau = 0$, let $h(x)$ be a smooth spatially heterogeneous toxicant input. Consider a smooth single-spike solution that remains localized on an $\mathcal{O}(\varepsilon)$ spatial scale and has a well-defined center $x_0(t)$. The dynamics of the spike center on the $\mathcal{O}(\varepsilon^2)$ time scale is governed by the reduced ordinary differential equation:*

$$\frac{dx_0}{dt} = -\frac{1}{\varepsilon^2}\bar{w}_x(x_0), \quad \textit{with} \quad D\bar{w}_{xx} + h(x) - \bar{w} = 0,\ \bar{w}_x(\pm\ell) = 0. \tag{1.9}$$

The asymptotic predictions are compared with numerical solutions of the time-dependent PDE in Figure 3, which illustrates the agreement between the numerically computed positions $x_0(t)$ and the corresponding reduced equations (1.6) and (1.9).

The two reductions reveal different drift scales. A weakly heterogeneous toxicant input produces spike motion on the $\mathcal{O}(\varepsilon)$ time scale, whereas an order-one heterogeneous input produces motion on the faster $\mathcal{O}(\varepsilon^2)$ time scale, governed at leading order by the gradient of the background toxicant concentration.

Another feature of the reduced dynamics is that the spike height is retained as an independent slow variable coupled to the fast motion of the spike center. In the weakly heterogeneous regime, its evolution is governed by (1.7), whereas in the strongly heterogeneous regime, it is determined by an implicit mass-balance equation (4.33) that involves the local spike profile. Previous matched-asymptotic studies of related chemotaxis systems typically determine the height of a steady spike through a solvability condition, but do not derive a separate time-dependent height equation coupled to the spike position. To our knowledge, this is the first such fast-slow reduction for a chemotaxis-type spike.

The remainder of this paper is organized as follows. In Section 2, we construct boundary spike solutions using matched asymptotic expansions and derive Proposition 1.1. In Section 3, we perform a formal spectral analysis for boundary and interior spike solutions and derive Proposition 1.2. In Section 4, we derive the reduced ODE systems governing the drift dynamics of spikes with weakly and strongly heterogeneous toxicant inputs, deriving Propositions 1.3 and 1.4, respectively. Numerical comparisons are also presented for representative parameter values. Finally, Section 5 contains a discussion of the results and directions for future research.

2 Construction of asymptotic spike solutions

In this section, we construct asymptotic spike solutions for (1.2). The construction is based on matched asymptotic expansions. We first derive the elementary half-spike profile on the interval $(0, \ell)$. This profile serves as the local building block for boundary spikes and, after even reflection across the spike center, for symmetric interior spikes. The resulting asymptotic profile is the one stated in Proposition 1.1.

Throughout this section, we assume that the toxicant input is spatially homogeneous, $h(x) \equiv h > 0$, and that the effective growth rate at the toxicant-only background level is positive: $r - mh > 0$. Since the toxicant-only state is $(0, h)$, it is natural to introduce the scaled variable $v = \frac{h-w}{\varepsilon}$. Then (u, v) satisfies:

$$\begin{cases} u_t = u_{xx} - \varepsilon^{-1}(uv_x)_x + u(r - mh + \varepsilon mv) - au^2, & x \in (-\ell, \ell), \\ \tau v_t = Dv_{xx} - v + \frac{bh}{\varepsilon}u - buv, & x \in (-\ell, \ell) \\ u_x(\pm\ell) = 0, \quad v_x(\pm\ell) = 0. \end{cases} \tag{2.1}$$

This system can be regarded as a perturbation to the Keller-Segel model with logistic growth, see [20].

Now we construct a steady-state solution of (2.1) in the form of a symmetric spike centered at the origin. Equivalently, this can be achieved by constructing a half-spike on the interval $(0, \ell)$ subject to Neumann boundary conditions, with the corresponding interior spike obtained by even reflection across the origin. The half-spike steady state therefore satisfies:

$$\begin{cases} 0 = u_{xx} - \varepsilon^{-1}(uv_x)_x + (u(r - mh + \varepsilon mv) - au^2), & x \in (0, \ell); \\ 0 = Dv_{xx} - v + \frac{bh}{\varepsilon}u - buv, & x \in (0, \ell), \\ u_x(0) = u_x(\ell) = 0, \quad v_x(0) = v_x(\ell) = 0. \end{cases} \tag{2.2}$$

The spike is centered at $x = 0$ and has spatial width of order $\mathcal{O}(\varepsilon)$.

• Inner region. We first analyze the region near the spike center $x = 0$. Introduce a local coordinate y such that $x = \varepsilon y$ and inner variable $U(y) = u(\varepsilon y)$, $V(y) = v(\varepsilon y)$. Then, letting $\varepsilon \to 0$, the interval $(0, \ell/\varepsilon)$ expands to $(0, \infty)$. System (2.2) becomes

$$\begin{cases} 0 = \varepsilon U_{yy} - (UV_y)_y + \varepsilon^3(U(r - mh + \varepsilon mV) - aU^2), & y \in (0, \infty), \\ 0 = DV_{yy} + \varepsilon bhU - \varepsilon^2 V - b\varepsilon^2 UV, & y \in (0, \infty), \\ U_y(0) = V_y(0) = 0. \end{cases} \tag{2.3}$$

We seek a localized spike profile of (2.3) satisfying $U(y) \to 0$ as $y \to \infty$. We expand

$$U(y) \sim U_0(y) + \varepsilon U_1(y) + \varepsilon^2 U_2(y) + \cdots, \quad V(y) \sim V_0(y) + \varepsilon V_1(y) + \varepsilon^2 V_2(y) + \cdots. \tag{2.4}$$

Substituting (2.4) into (2.3) and collecting powers of ε, we obtain the following hierarchy of problems for (U_j, V_j) on the half-line $(0, \infty)$. For each inner problem below, the symmetry conditions are imposed at $y = 0$. The component U_j is required to be localized as $y \to +\infty$, whereas the far-field behavior of V_j is not prescribed independently but is determined by matching with the corresponding outer expansion. Whenever needed, these matching conditions are stated explicitly below.

1. Collecting terms at order $\mathcal{O}(1)$, we obtain

$$\begin{cases} (U_0 V_{0y})_y = 0, & y \in (0, \infty), \\ DV_{0yy} = 0, & y \in (0, \infty), \\ U_{0y}(0) = V_{0y}(0) = 0, \end{cases} \tag{2.5}$$

We seek a solution to (2.5) with V_0 bounded as $y \to \infty$. Then solving (2.5) yields

$$V_0 = C_0, \tag{2.6}$$

where C_0 is a constant to be determined by matching with the solution in the outer region.

2. Collecting terms of order $\mathcal{O}(\varepsilon)$, we obtain:

$$\begin{cases} U_{0yy} - (U_0 V_{1y})_y = 0, & y \in (0,\infty), \\ DV_{1yy} + bhU_0 = 0, & y \in (0,\infty), \\ U_{0y}(0) = V_{1y}(0) = 0. \end{cases} \tag{2.7}$$

Solving the first equation with $U_{0y}(\infty) = 0$, integration yields

$$U_{0y} - U_0 V_{1y} = 0 \tag{2.8}$$

which yields

$$U_0(y) = Ae^{V_1(y)}, \quad y \in (0,\infty), \tag{2.9}$$

where A is a constant to be determined. Plugging (2.9) into the second equation of (2.7) yields

$$DV_{1yy} + bhAe^{V_1} = 0, \quad y \in (0,\infty); \quad V_{1y}(0) = 0.$$

This is a Liouville-type equation on the half-line with the symmetry condition $V_{1y}(0) = 0$. Equivalently, V_1 is obtained by restricting an even whole-line solution to $y > 0$. Thus

$$V_1(y) = \ln\left(\frac{\mu}{2}\mathrm{sech}^2\left(\frac{\sqrt{\mu}}{2}\sqrt{\frac{bhA}{D}}y\right)\right), \quad y \in (0,\infty), \tag{2.10}$$

where μ is a constant to be determined. Then (2.9) becomes

$$U_0(y) = \frac{\mu A}{2}\,\mathrm{sech}^2\left(\sqrt{\frac{\mu Abh}{4D}}\,y\right), \quad y \in (0,\infty). \tag{2.11}$$

The far-field behaviors of V_1 are

$$V_1 \sim \ln(2\mu) - \sqrt{\frac{\mu bhA}{D}}y \quad \text{and} \quad V_{1y} \to -\sqrt{\frac{\mu bhA}{D}}, \quad \text{as } y \to +\infty. \tag{2.12}$$

3. At order $\mathcal{O}(\varepsilon^2)$, we obtain:

$$\begin{cases} U_{1yy} - (U_0 V_{2y} + U_1 V_{1y})_y = 0, & y \in (0,\infty), \\ DV_{2yy} - V_0 - bU_0 V_0 + bhU_1 = 0, & y \in (0,\infty), \\ U_{1y}(0) = V_{2y}(0) = 0, \quad U_1(y) \to 0, \ (y \to \infty), \end{cases} \tag{2.13}$$

From the first equation in (2.13) along with (2.8), it follows that $\left(\frac{U_1}{U_0}\right)_y = V_{2y}$. This gives

$$U_1 = (V_2 + A_1)U_0, \tag{2.14}$$

where A_1 is a constant to be determined. Plugging (2.14) back into the second equation in (2.13), together with (2.6), we obtain

$$DV_{2yy} + bhV_2U_0 = C_0 + b(C_0 - hA_1)U_0, \quad V_{2y}(0) = 0. \tag{2.15}$$

A convenient representation of V_2 is

$$V_2 = -C_1\left(A\frac{\partial V_1}{\partial A} + 1\right) + C_0\left(F(y) + \frac{y^2}{2D} + \frac{1}{h}\right) - A_1, \tag{2.16}$$

where C_1 is a constant to be determined and $F(y)$ satisfies

$$DF_{yy} + bhU_0F = -\frac{bhy^2U_0}{2D}, \quad F_y(0) = 0, \ F_y(\infty) = 0. \tag{2.17}$$

Equation (2.17) generally has to be solved numerically. By (2.16) and (2.12), the far-field behavior of V_2 is

$$V_2 \sim \frac{C_0 y^2}{2D} + \frac{C_1}{2}\sqrt{\frac{\mu b h A}{D}}y + \frac{C_0}{h} - A_1 - C_1 + C_0 F(\infty) \quad \text{as } y \to +\infty. \tag{2.18}$$

Since A_1 is an undetermined additive constant, the constant $C_0F(\infty)$ may be absorbed into A_1. We shall use this convention in the matching below.

4. At order $\mathcal{O}(\varepsilon^3)$, the equation for U_2 is

$$U_{2yy} - (U_0V_{3y} + U_2V_{1y})_y = (U_1V_{2y})_y - \left((r-mh)U_0 - aU_0^2\right), \quad U_{2y}(0) = 0,\ U_{2y}(\infty) = 0. \tag{2.19}$$

Integrating the first equation of (2.19) over $(0,\infty)$ gives the solvability condition:

$$\int_0^\infty U_0(r - mh - aU_0)\mathrm{d}y = 0. \tag{2.20}$$

Since

$$\int_0^\infty \operatorname{sech}^2(ky)\,\mathrm{d}y = \frac{1}{k}, \qquad \int_0^\infty \operatorname{sech}^4(ky)\,\mathrm{d}y = \frac{2}{3k},$$

substituting (2.11) into (2.20), we obtain

$$\bar{A} := \frac{1}{2}\mu A = \frac{(r-mh)\int_0^\infty \operatorname{sech}^2(y\sqrt{\frac{\mu A b h}{4D}})\mathrm{d}y}{a\int_0^\infty \operatorname{sech}^4(y\sqrt{\frac{\mu A b h}{4D}})\mathrm{d}y} = \frac{3(r-mh)}{2a}. \tag{2.21}$$

5. At order $\mathcal{O}(\varepsilon^4)$, U_3 satisfies

$$\begin{aligned} &U_{3yy} - (U_0V_{4y} + U_3V_{1y})_y = (U_1V_{3y} + U_2V_{2y})_y - \left((r-mh)U_1 - 2aU_0U_1 + mC_0U_0\right), \\ &U_{3y}(0) = 0,\ U_{3y}(\infty) = 0. \end{aligned} \tag{2.22}$$

Integrating the first equation of (2.22) over $(0,\infty)$, we obtain the solvability condition:

$$\int_0^\infty \big((r-mh)U_1 - 2aU_0U_1 + mC_0U_0\big)\mathrm{d}y = 0. \tag{2.23}$$

Plugging (2.14) and (2.16) into (2.23), we obtain

$$\begin{aligned} 0 = &\int_0^\infty \big((r-mh) - 2aU_0\big)U_0\left[-C_1\left(A\frac{\partial V_1}{\partial A} + 1\right) + C_0\left(F(y) + \frac{y^2}{2D} + \frac{1}{h}\right)\right]\mathrm{d}y \\ &+ mC_0\int_0^\infty U_0\,\mathrm{d}y, \end{aligned} \tag{2.24}$$

which gives

$$C_1 = \kappa C_0, \quad \text{with} \quad \kappa := \frac{\int_0^\infty \left[\big((r-mh) - 2aU_0\big)U_0\left(F(y) + \frac{y^2}{2D} + \frac{1}{h}\right) + mU_0\right]\mathrm{d}y}{\int_0^\infty \big((r-mh) - 2aU_0\big)U_0\left(A\frac{\partial V_1}{\partial A} + 1\right)\mathrm{d}y}. \tag{2.25}$$

• Outer region. In the outer region, where x is separated from the spike center by a distance much larger than ε, the population component u is exponentially small. Then the terms $\frac{bh}{\varepsilon}u$ and buv in the v-equation are exponentially small away from the spike core. Therefore, the leading-order outer field, denoted by v_{out}, satisfies

$$\begin{cases} D(v_{\text{out}})_{xx} - v_{\text{out}} = 0, & 0 < x < \ell, \\ (v_{\text{out}})_x(\ell) = 0. \end{cases} \tag{2.26}$$

No boundary condition is imposed at $x = 0$ on the outer problem. Indeed, the Neumann condition at the spike center is satisfied through the inner correction, whereas the nonzero one-sided derivative of the outer solution at $x = 0$ is determined by matching with the far-field behavior of the inner solution.

The solution of (2.26) has the form

$$v_{\text{out}}(x) = B\cosh\left(\frac{\ell - x}{\sqrt{D}}\right),$$

where B is an undetermined constant. For convenience in the subsequent matching calculation, we write $v_{\text{out}}(x) = sG(x)$, where s is to be determined and G is the Green function satisfying

$$\begin{cases} DG_{xx} - G = 0, & 0 < x < \ell, \\ G_x(0^+) = -\dfrac{1}{2}, \qquad G_x(\ell) = 0. \end{cases} \tag{2.27}$$

Solving (2.27), we obtain

$$G(x) = \frac{\sqrt{D}}{2\sinh\left(\ell/\sqrt{D}\right)}\cosh\left(\frac{\ell - x}{\sqrt{D}}\right), \qquad 0 \le x \le \ell. \tag{2.28}$$

In particular,

$$G(0) = \frac{\sqrt{D}}{2}\coth\left(\frac{\ell}{\sqrt{D}}\right), \qquad G_x(0^+) = -\frac{1}{2}, \qquad G_{xx}(0^+) = \frac{G(0)}{D}. \tag{2.29}$$

• Matching and determination of the constants. We now determine the constants C_0 and μ in the inner expansion and the amplitude s in the outer expansion by matching the local behavior of the outer solution near $x = 0$ with the far-field behavior of the inner solution.

We first expand the outer amplitude as

$$s \sim s_0 + \varepsilon s_1 + \varepsilon^2 s_2 + \cdots. \tag{2.30}$$

In the matching region $1 \ll y \ll \varepsilon^{-1}, x = \varepsilon y$, the outer solution satisfies

$$\begin{aligned} v_{\text{out}}(\varepsilon y) &\sim \left(s_0 + \varepsilon s_1 + \varepsilon^2 s_2 + \cdots\right)\left[G(0) + \varepsilon G_x(0^+)y + \varepsilon^2\frac{G_{xx}(0^+)}{2}y^2 + \cdots\right] \\ &\sim s_0 G(0) + \varepsilon\left[s_0 G_x(0^+)y + s_1 G(0)\right] \\ &\quad + \varepsilon^2\left[\frac{s_0 G_{xx}(0^+)}{2}y^2 + s_1 G_x(0^+)y + s_2 G(0)\right] + \cdots. \end{aligned} \tag{2.31}$$

We next determine the far-field expansion of the inner solution. By (2.12),

$$V_1(y) \sim -\sqrt{\frac{\mu bhA}{D}}\,y + \ln(2\mu) \qquad \text{as } y \to +\infty. \tag{2.32}$$

Moreover, differentiating (2.10) with respect to A gives

$$A\frac{\partial V_1}{\partial A} = -\frac{1}{2}\sqrt{\frac{\mu bhA}{D}}\,y\tanh\left(\frac{1}{2}\sqrt{\frac{\mu bhA}{D}}\,y\right). \tag{2.33}$$

Hence,

$$A\frac{\partial V_1}{\partial A} + 1 = 1 - \frac{1}{2}\sqrt{\frac{\mu bhA}{D}}\,y + o(1) \qquad \text{as } y \to +\infty. \tag{2.34}$$

Using (2.16), (2.34), and $F(y) \to F(\infty)$ as $y \to +\infty$, we obtain

$$V_2(y) \sim \frac{C_0}{2D} y^2 + \frac{C_1}{2}\sqrt{\frac{\mu bhA}{D}}\, y + \frac{C_0}{h} - A_1 - C_1 + C_0 F(\infty) \quad \text{as } y \to +\infty. \tag{2.35}$$

Therefore, the far-field behavior of the inner expansion is

$$\begin{aligned} V(y) \sim C_0 &+ \varepsilon \left[-\sqrt{\frac{\mu bhA}{D}}\, y + \ln(2\mu) \right] \\ &+ \varepsilon^2 \left[\frac{C_0}{2D} y^2 + \frac{C_1}{2}\sqrt{\frac{\mu bhA}{D}}\, y + \frac{C_0}{h} - A_1 - C_1 + C_0 F(\infty) \right] + \cdots . \end{aligned} \tag{2.36}$$

Matching the terms of (2.31) and (2.36) at each order of ε, we obtain

$$\begin{aligned} &\mathcal{O}(1): \quad s_0 G(0) = C_0, \\ &\mathcal{O}(\varepsilon): \quad s_0 G_x(0^+) = -\sqrt{\frac{\mu bhA}{D}},\ s_1 G(0) = \ln(2\mu), \\ &\mathcal{O}(\varepsilon^2): \quad \frac{s_0 G_{xx}(0^+)}{2} = \frac{C_0}{2D},\ s_1 G_x(0^+) = \frac{C_1}{2}\sqrt{\frac{\mu bhA}{D}}, \\ &\qquad\qquad s_2 G(0) = \frac{C_0}{h} - A_1 - C_1 + C_0 F(\infty). \end{aligned} \tag{2.37}$$

The first matching condition at order $\mathcal{O}(\varepsilon^2)$ is automatically satisfied. Indeed, $G_{xx}(0^+) = \frac{G(0)}{D}$ by (2.29), and hence, using $s_0 G(0) = C_0$, we have $s_0 G_{xx}(0^+) = \frac{s_0 G(0)}{D} = \frac{C_0}{D}$. Then the matching condition (2.37) yields

$$\begin{aligned} &s_0 = 2\sqrt{\frac{\mu bhA}{D}}, \quad C_0 = \sqrt{\mu bhA}\coth\left(\frac{\ell}{\sqrt{D}}\right), \\ &s_1 = -C_1\sqrt{\frac{\mu bhA}{D}}, \quad \ln 2\mu = \frac{s_1\sqrt{D}}{2}\coth\left(\frac{\ell}{\sqrt{D}}\right). \end{aligned} \tag{2.38}$$

Combining (2.38), (2.21) and (2.25), we obtain

$$s_0 = 2\sqrt{\frac{2bh\bar{A}}{D}}, \quad C_0 = \sqrt{2bh\bar{A}}\coth\left(\frac{\ell}{\sqrt{D}}\right), \quad s_1 = -\sqrt{\frac{2bh\bar{A}}{D}}C_1, \quad C_1 = \kappa C_0, \tag{2.39}$$

where $\bar{A} = \frac{3(r-mh)}{2a}$ from (2.21).

Finally, substituting $C_1 = \kappa C_0$ into the third matching condition in (2.37), we find that μ is determined by

$$\ln(2\mu) = -\kappa bh\bar{A}\coth^2\left(\frac{\ell}{\sqrt{D}}\right). \tag{2.40}$$

Equivalently,

$$\mu = \frac{1}{2}\exp\left[-\kappa bh\bar{A}\coth^2\left(\frac{\ell}{\sqrt{D}}\right)\right]. \tag{2.41}$$

Although μ is required to close the higher-order inner expansion, it does not appear explicitly in the leading spike profile because $\mu A = 2\bar{A}$.

We then use Van Dyke's matching principle to obtain the composite expansion of w_s. Indeed, by using $v_{\rm s} = V_{\rm inner} + v_{\rm outer} - V_{\rm overlap}$, we have the following uniform asymptotic expansion of the equilibrium state of (1.2):

$$\begin{aligned} &u_s(x) \sim \bar{A}\,\mathrm{sech}^2\left(\sqrt{\frac{\bar{A}bh}{2D}}\frac{x}{\varepsilon}\right), \\ &w_s(x) \sim h - \varepsilon v_s(x), \\ &\text{where} \quad v_s(x) = s_0 G(x) + \varepsilon\left(s_1 G(x) + \ln\left(\mathrm{sech}^2\left(\sqrt{\frac{\bar{A}bh}{2D}}\frac{x}{\varepsilon}\right)\right) + \sqrt{\frac{2\bar{A}bh}{D}}\frac{x}{\varepsilon} - 2\ln 2\right). \end{aligned} \tag{2.42}$$

This completes the formal construction of the half-spike profile stated in Proposition 1.1.

Remark 1. The construction of the boundary spike follows the Type I spike construction in [20]. However, we provide a more detailed description of the higher-order terms of v. In particular, the higher-order solvability condition determines the constant κ in (2.25), and the remaining matching condition determines μ. These constants are required to close the matching calculation and to obtain the toxicant profile through order $\mathcal{O}(\varepsilon^2)$.

3 Stability: stable boundary spikes and unstable interior spikes

Building on the results established in Section 2, we now carry out a formal spectral analysis for the boundary and interior spike equilibria. We linearize system (2.1) about the corresponding formal steady-state profiles and distinguish the relevant eigenvalues according to their asymptotic size and the parity of their eigenfunctions.

For the boundary spike, we first consider eigenvalues of order $\mathcal{O}(\varepsilon^{-2})$ and show that the corresponding leading-order eigenvalue problem only has eigenvalues with negative real parts. We then examine the relevant $\mathcal{O}(1)$ structural mode and derive an asymptotic formula showing that its eigenvalue is negative. By contrast, the interior spike admits an additional odd translational mode, and we show that the associated eigenvalue is positive.

The essential difference between the two cases is therefore the presence of the translational mode. This mode is excluded for the boundary half-spike by the symmetry condition at the spike center, whereas for an interior spike it is admissible and its eigenvalue is determined through the coupling between the inner translational mode and the outer solution.

3.1 Stability of a boundary spike

We now perform a formal linear stability analysis of the boundary spike constructed in Section 2. Let (u_s, v_s) denote the corresponding steady-state profile of system (2.1) defined in (2.42). Linearizing system (2.1) at (u_s, v_s), we obtain

$$\begin{cases} \lambda\phi = \phi_{xx} - \varepsilon^{-1}\big(\phi v_{s,x} + u_s\psi_x\big)_x + \big(r - mh - 2au_s\big)\phi + \varepsilon m\big(u_s\psi + v_s\phi\big), & 0 < x < \ell, \\ \tau\lambda\psi = D\psi_{xx} - \psi + \frac{bh}{\varepsilon}\phi - b\big(u_s\psi + v_s\phi\big), & 0 < x < \ell, \\ \phi_x(0) = \psi_x(0) = \phi_x(\ell) = \psi_x(\ell) = 0, \end{cases} \tag{3.1}$$

where $\lambda \in \mathbb{C}$ is the spectral parameter and $(\phi, \psi) \not\equiv (0, 0)$ is the corresponding eigenfunction.

The eigenfunctions can first be separated into "spike-core" mode and "purely toxicant" mode according to whether the ϕ-component is localized at the leading order. By spike-core modes, we mean eigenfunctions for which ϕ has a nontrivial leading-order structure within the $\mathcal{O}(\varepsilon)$ neighborhood of the boundary spike. Their eigenvalues must therefore be determined through a coupled inner-outer analysis. In contrast, for the purely toxicant outer modes, their ϕ-component is negligible to leading order, with $\phi \sim 0$ in both the inner and outer regions. The system (3.1) at the leading order reduces to

$$\tau\lambda\psi = D\psi_{xx} - \psi, \ x \in (0, \ell)$$

subject to the homogeneous Neumann boundary conditions. When $\tau > 0$, the corresponding eigenvalues are real and strictly negative for every fixed spatial mode. When $\tau = 0$, the equation for ψ is an elliptic constraint and generates no independent temporal eigenvalues. These purely toxicant modes therefore cannot destabilize the boundary spike.

It remains to analyze the spike-core modes. Directly integrating the first equation of (3.1) over $(0, \ell)$ yields the following solvability condition

$$\lambda \int_0^\ell \phi \, \mathrm{d}x = \int_0^\ell \left(r - mh - 2au_s\right)\phi \, \mathrm{d}x + \varepsilon m \int_0^\ell \left(u_s\psi + v_s\phi\right) \mathrm{d}x. \tag{3.2}$$

This identity will be useful later in determining the small eigenvalue regime. However, the size of $\int_0^\ell \phi \, \mathrm{d}x$ alone does not determine the asymptotic magnitude of λ, since the right-hand side of (3.2) may have the same asymptotic order or may vanish simultaneously. The relevant spectral scales are therefore identified from the dominant balances in the inner region.

As shown below, their dominant inner balances give rise to the two distinguished eigenvalue scales $\mathcal{O}(\varepsilon^{-2})$ and $\mathcal{O}(1)$.

In the inner region: near the spike center $x = 0$, we rescale $x = \varepsilon y$ and let

$$\Phi(y) = \phi(\varepsilon y), \qquad \Psi(y) = \psi(\varepsilon y). \tag{3.3}$$

Recall that $(U(y), V(y)) = (u_s(\varepsilon y), v_s(\varepsilon y))$ denotes the inner representation of the boundary-spike steady state constructed in Section 2. Then letting $\varepsilon \to 0$, the interval $(0, \ell/\varepsilon)$ expands to $(0, \infty)$, and problem (3.1) becomes

$$\begin{cases} \varepsilon^3 \lambda \Phi = \varepsilon \Phi_{yy} - \big(\Phi V_y + U \Psi_y\big)_y + \varepsilon^3 \big(r - mh - 2aU\big)\Phi + m\varepsilon^4 \big(U\Psi + V\Phi\big), & y \in (0, \infty), \\ \tau \varepsilon^2 \lambda \Psi = D \Psi_{yy} + \varepsilon b h \Phi - \varepsilon^2 \Psi - b\varepsilon^2 \big(U\Psi + V\Phi\big), & y \in (0, \infty), \\ \Phi_y(0) = \Psi_y(0) = 0, \quad \Phi(\infty) = 0. \end{cases} \tag{3.4}$$

The inner eigenvalue problem (3.4) suggests two distinguished spectral scales. In particular, when $\tau > 0$, the second equation of (3.4) contains the balance

$$\tau \varepsilon^2 \lambda \Psi \quad \text{and} \quad D \Psi_{yy}.$$

Since the diffusion term $D\Psi_{yy}$ is of order $\mathcal{O}(1)$ in the inner variable, this balance allows eigenvalues as large as of order $\mathcal{O}(\varepsilon^{-2})$. Thus, we study (3.4) by splitting the discussion into two types of eigenvalues: the large eigenvalues of order $\mathcal{O}(\varepsilon^{-2})$ and the small eigenvalues of order $\mathcal{O}(1)$.

3.1.1 Large eigenvalues

We first focus on large eigenvalues of order $\mathcal{O}(\varepsilon^{-2})$, whose corresponding leading-order eigenfunctions are localized in the inner region near the spike. We seek an asymptotic expansion of the form

$$\lambda = \varepsilon^{-2}(\lambda_{la} + \mathcal{O}(\varepsilon)), \qquad \lambda_{la} \neq 0$$

In the outer region: away from the spike center, the steady-state population component u_s is exponentially small. If $\tau > 0$, multiplying the first two equations in (3.1) by ε^2 and retaining the leading-order terms gives

$$\lambda_{la} \phi \sim 0, \quad \tau \lambda_{la} \psi \sim 0.$$

Since we are interested in nontrivial eigenvalues satisfying $\lambda_{la} \neq 0$, it follows that $\phi \sim 0$ and $\psi \sim 0$ to leading order in the outer region. Therefore, the leading-order eigenfunctions are localized near the spike center, and the corresponding eigenvalue problem is determined by the inner region.

When $\tau = 0$, the ψ equation is elliptic. In this case, the leading inner ψ component may be a constant determined by matching with the outer solution. This constant does not enter the ϕ equation, since only derivatives of Ψ occur there. After absorbing it into the leading outer value, the first nonconstant inner correction is again governed by (3.8), with $\tau = 0$.

In the inner region: near the spike center, we obtain for $y \in (0, \infty)$

$$\begin{cases} \lambda_{la} \varepsilon \Phi = \varepsilon \Phi_{yy} - (\Phi V_y + U \Psi_y)_y + \varepsilon^3 \left((r - mh) - 2aU\right) \Phi + m\varepsilon^4 (U\Psi + V\Phi), \\ \tau \lambda_{la} \Psi = D \Psi_{yy} + \varepsilon b h \Phi - \varepsilon^2 \Psi - b\varepsilon^2 (U\Psi + V\Phi), \\ \Phi_y(0) = \Psi_y(0) = 0, \quad \Phi(\infty) = \Psi(\infty) = 0. \end{cases} \tag{3.5}$$

We seek formal asymptotic expansions of the eigenfunctions in the form

$$\Phi \sim \Phi_0 + \varepsilon\Phi_1 + \varepsilon^2\Phi_2 + \cdots, \quad \Psi \sim \Psi_0 + \varepsilon\Psi_1 + \varepsilon^2\Psi_2 + \cdots. \tag{3.6}$$

Substituting (3.6), together with the steady-state expansions

$$U \sim U_0 + \varepsilon U_1 + \cdots, \qquad V \sim V_0 + \varepsilon V_1 + \cdots,$$

into (3.5) and comparing the equations at each order of ε, we obtain the following hierarchy of equations.

At order $\mathcal{O}(1)$, recalling that $V_0 = C_0$ is a constant, we obtain

$$\begin{cases} (U_0\Psi_{0y})_y = 0, & y \in (0,\infty) \\ D\Psi_{0yy} = \tau\lambda_{la}\Psi_0. & y \in (0,\infty) \\ \Phi_{0y}(0) = \Psi_{0y}(0) = 0, \quad \Phi_0(\infty) = \Psi_0(\infty) = 0. \end{cases} \tag{3.7}$$

The first equation of (3.7), together with $\Psi_{0y}(0) = 0$ and $U_0 > 0$, gives $\Psi_{0y} \equiv 0$. Hence Ψ_0 is constant. Since the eigenfunction corresponding to large eigenvalue is localized in the inner region, the far-field condition $\Psi_0(\infty) = 0$ implies

$$\Psi_0 \equiv 0.$$

The function Φ_0 and the coefficient λ_{la} are determined by the next-order problem.

At order $\mathcal{O}(\varepsilon)$, using $\Psi_0 \equiv 0$, we obtain

$$\begin{cases} \lambda_{la}\Phi_0 = \Phi_{0yy} - (\Phi_0 V_{1y} + U_0\Psi_{1y})_y, & y \in (0,\infty), \\ \tau\lambda_{la}\Psi_1 = D\Psi_{1yy} + bh\Phi_0, & y \in (0,\infty), \\ \Phi_{0y}(0) = \Psi_{1y}(0) = 0, \ \Phi_0(\infty) = 0, \ \Psi_1(\infty) = 0. \end{cases} \tag{3.8}$$

Thus the leading coefficient λ_{la} of the large eigenvalue is determined by the half-line spectral problem (3.8). We characterize its sign in the following theorem.

Theorem 3.1. *Consider the eigenvalue problem*

$$\begin{cases} \lambda_{la}\Phi_0 = \Phi_{0yy} - \big(\Phi_0 V_{1y} + U_0\Psi_{1y}\big)_y, & y \in (0,\infty), \\ \tau\lambda_{la}\Psi_1 = D\Psi_{1yy} + bh\Phi_0, & y \in (0,\infty), \\ \Phi_{0y}(0) = \Psi_{1y}(0) = 0, \qquad \Phi_0(\infty) = \Psi_1(\infty) = 0, \end{cases} \tag{3.9}$$

where

$$U_0(y) = \bar{A}\operatorname{sech}^2\left(\sqrt{\frac{\bar{A}bh}{2D}}\, y\right), \qquad V_{1y} = \frac{U_{0y}}{U_0}, \qquad \tau \geq 0.$$

Then (3.9) *has no nonzero eigenvalue* λ_{la} *satisfying* $\operatorname{Re}\lambda_{la} \geq 0$.

Proof. Suppose, to the contrary, that

$$\operatorname{Re}\lambda_{la} \geq 0, \qquad \lambda_{la} \neq 0.$$

We first justify the far-field conditions needed below. Set $\kappa := \sqrt{\frac{\bar{A}bh}{2D}}$. As $y \to \infty$, we have

$$U_0(y) \sim 4\bar{A}e^{-2\kappa y}, \qquad V_{1y}(y) \to -2\kappa, \qquad V_{1yy}(y) \to 0.$$

Since U_0 is exponentially small, the leading far-field equation for Φ_0 is

$$\lambda_{la}\Phi_0 \sim \Phi_{0yy} + 2\kappa\Phi_{0y}.$$

The corresponding characteristic exponents are

$$\rho_\pm = -\kappa \pm \sqrt{\kappa^2 + \lambda_{la}},$$

where the square root is chosen to have positive real part.

We claim that

$$\operatorname{Re}\sqrt{\kappa^2 + \lambda_{la}} > \kappa.$$

Indeed, write

$$\sqrt{\kappa^2 + \lambda_{la}} = \alpha + i\beta, \qquad \alpha > 0.$$

Then

$$\alpha^2 - \beta^2 = \kappa^2 + \operatorname{Re}\lambda_{la} \geq \kappa^2.$$

Hence $\alpha \geq \kappa$. Equality would imply $\beta = 0$ and $\lambda_{la} = 0$, which is excluded. Therefore $\alpha > \kappa$.

The decay condition on Φ_0 selects the exponent ρ_-. Consequently,

$$\frac{\Phi_0(y)}{U_0(y)} = O\left(e^{-(\alpha-\kappa)y}\right) \longrightarrow 0 \qquad \text{as } y \to \infty.$$

The lower-order term involving $U_0\Psi_{1y}$ does not change this leading far-field behavior because U_0 and Ψ_1 decay at infinity. The second equation in (3.9), together with the decay of Φ_0 and Ψ_1, gives the corresponding decay of Ψ_{1y}. A variation-of-constants argument in the first equation then shows that the term involving $U_0\Psi_{1y}$ does not alter the decaying far-field branch. Consequently,

$$\Theta_0(y) := U_0^{-1}\Phi_0 - \Psi_1 \longrightarrow 0 \qquad \text{as } y \to \infty.$$

The same far-field estimates show that all the integrals below are finite and that the boundary terms arising from integration by parts vanish.

Using

$$\Phi_0 = U_0(\Theta_0 + \Psi_1), \qquad V_{1y} = \frac{U_{0y}}{U_0},$$

we rewrite (3.9) as

$$\begin{cases} \lambda_{la} U_0(\Theta_0 + \Psi_1) = (U_0\Theta_{0y})_y, \\ \tau\lambda_{la}\Psi_1 = D\Psi_{1yy} + bhU_0(\Theta_0 + \Psi_1), \\ \Theta_{0y}(0) = \Psi_{1y}(0) = 0, \qquad \Theta_0(\infty) = \Psi_1(\infty) = 0. \end{cases} \tag{3.10}$$

Multiplying the first and second equations of (3.10) by $\overline{\Theta}_0$ and $\overline{\Psi}_1$, respectively, and integrating over $(0,\infty)$, we obtain

$$\begin{cases} \lambda_{la}\left(\displaystyle\int_0^\infty U_0|\Theta_0|^2\,\mathrm{d}y + \int_0^\infty U_0\Psi_1\overline{\Theta}_0\,\mathrm{d}y\right) = -\int_0^\infty U_0|\Theta_{0y}|^2\,\mathrm{d}y, \\ \tau\lambda_{la}\displaystyle\int_0^\infty |\Psi_1|^2\,\mathrm{d}y = -D\int_0^\infty |\Psi_{1y}|^2\,\mathrm{d}y + bh\int_0^\infty U_0|\Psi_1|^2\,\mathrm{d}y + bh\int_0^\infty U_0\Theta_0\overline{\Psi}_1\,\mathrm{d}y. \end{cases} \tag{3.11}$$

Taking the complex conjugate of the second equation gives

$$\int_0^\infty U_0\Psi_1\overline{\Theta}_0\,\mathrm{d}y = \frac{1}{bh}\left(\tau\overline{\lambda}_{la}\int_0^\infty |\Psi_1|^2\,\mathrm{d}y + D\int_0^\infty |\Psi_{1y}|^2\,\mathrm{d}y - bh\int_0^\infty U_0|\Psi_1|^2\,\mathrm{d}y\right). \tag{3.12}$$

Substituting (3.12) into the first equation of (3.11), we obtain

$$\lambda_{la}\mathcal{K} + \tau|\lambda_{la}|^2\int_0^\infty |\Psi_1|^2\,\mathrm{d}y = -bh\int_0^\infty U_0|\Theta_{0y}|^2\,\mathrm{d}y, \tag{3.13}$$

where

$$\mathcal{K} := bh\int_0^\infty U_0|\Theta_0|^2\,\mathrm{d}y + D\int_0^\infty |\Psi_{1y}|^2\,\mathrm{d}y - bh\int_0^\infty U_0|\Psi_1|^2\,\mathrm{d}y. \tag{3.14}$$

We next show that $\mathcal{K} > 0$ for every nontrivial eigenfunction. Integrating the first equation of (3.9) over $(0, \infty)$ and using $\lambda_{la} \neq 0$ gives

$$\int_0^\infty \Phi_0 \, \mathrm{d}y = 0. \tag{3.15}$$

Since $\Phi_0 = U_0(\Theta_0 + \Psi_1)$, we obtain

$$\int_0^\infty U_0 \Theta_0 \, \mathrm{d}y = -\int_0^\infty U_0 \Psi_1 \, \mathrm{d}y. \tag{3.16}$$

By the Cauchy–Schwarz inequality,

$$\left| \int_0^\infty U_0 \Theta_0 \, \mathrm{d}y \right|^2 \leq \left(\int_0^\infty U_0 \, \mathrm{d}y \right) \left(\int_0^\infty U_0 |\Theta_0|^2 \, \mathrm{d}y \right).$$

Combining this inequality with (3.16) yields

$$bh \int_0^\infty U_0 |\Theta_0|^2 \, \mathrm{d}y \geq \frac{bh}{\displaystyle\int_0^\infty U_0 \, \mathrm{d}y} \left| \int_0^\infty U_0 \Psi_1 \, \mathrm{d}y \right|^2. \tag{3.17}$$

Therefore,

$$\mathcal{K} \geq D \int_0^\infty |\Psi_{1y}|^2 \, \mathrm{d}y - bh \int_0^\infty U_0 |\Psi_1|^2 \, \mathrm{d}y + \frac{bh}{\displaystyle\int_0^\infty U_0 \, \mathrm{d}y} \left| \int_0^\infty U_0 \Psi_1 \, \mathrm{d}y \right|^2. \tag{3.18}$$

Let

$$z = \sqrt{\frac{\bar{A}bh}{2D}}\, y, \qquad \widehat{\Psi}_1(z) = \Psi_1 \left(\sqrt{\frac{2D}{\bar{A}bh}}\, z \right).$$

Since $U_0(y) = \bar{A} \operatorname{sech}^2 z$, a direct change of variables in (3.18) gives

$$\mathcal{K} \geq \sqrt{\frac{\bar{A}bhD}{2}}\, Q[\widehat{\Psi}_1], \tag{3.19}$$

where

$$Q[f] := \int_0^\infty |f_z|^2 \, \mathrm{d}z - \int_0^\infty 2 \operatorname{sech}^2 z \, |f|^2 \, \mathrm{d}z + \frac{1}{\displaystyle\int_0^\infty 2 \operatorname{sech}^2 z \, \mathrm{d}z} \left| \int_0^\infty 2 \operatorname{sech}^2 z \, f(z) \, \mathrm{d}z \right|^2. \tag{3.20}$$

By Lemma A.1, $Q[f] \geqq 0$, with equality if and only if $f \equiv 0$.

If $\Psi_1 \not\equiv 0$, then $Q[\widehat{\Psi}_1] > 0$, and hence $\mathcal{K} > 0$. If $\Psi_1 \equiv 0$, then

$$\mathcal{K} = bh \int_0^\infty U_0 |\Theta_0|^2 \, \mathrm{d}y.$$

For a nontrivial eigenfunction, $\Theta_0 \not\equiv 0$, so again $\mathcal{K} > 0$.

Taking the imaginary part of (3.13) gives $\operatorname{Im}(\lambda_{la})\mathcal{K} = 0$. Since $\mathcal{K} > 0$, we obtain $\operatorname{Im} \lambda_{la} = 0$. Thus λ_{la} is real. Since $\operatorname{Re} \lambda_{la} \geq 0$ and $\lambda_{la} \neq 0$, we must have $\lambda_{la} > 0$. However, the left-hand side of (3.13) is then strictly positive, whereas its right-hand side is nonpositive. This is a contradiction. Therefore, (3.9) has no nonzero eigenvalue in the closed right half-plane. □

3.1.2 Small eigenvalues

We now consider the $\mathcal{O}(1)$ eigenvalue. The analysis below follows the procedure used for the even eigenvalue of the Type I spike in [20, Sec. 2.2]: the leading-order eigenfunction is obtained from the scaling invariance of the inner problem, and the eigenvalue is then determined by an appropriate solvability condition.

In the inner region: near the spike center, we consider the inner eigenvalue problem (3.4). We expand

$$\lambda \sim \lambda_e + \varepsilon\lambda_1 + \cdots, \ \Phi \sim \Phi_0 + \varepsilon\Phi_1 + \varepsilon^2\Phi_2 + \cdots, \ \Psi \sim \Psi_0 + \varepsilon\Psi_1 + \varepsilon^2\Psi_2 + \cdots. \tag{3.21}$$

Substituting (3.21) into the system (3.4) and collecting the equations at each order of ε, we obtain the following hierarchy of equations.

At $\mathcal{O}(1)$, we obtain

$$\begin{cases} (\Phi_0 V_{0y} + U_0\Psi_{0y})_y = 0, & y \in (0,\infty), \\ D\Psi_{0yy} = 0, & y \in (0,\infty), \\ \Phi_{0y}(0) = \Psi_{0y}(0) = 0. \end{cases} \tag{3.22}$$

Since V_0 is constant and Ψ_0 is required to remain bounded as $y \to \infty$, the second equation of (3.22) gives

$$\Psi_0(y) = \text{constant}, \quad y \in (0,\infty). \tag{3.23}$$

Consequently, the first equation of (3.22) is identically satisfied and imposes no condition on Φ_0 at this order. The constant value of Ψ_0 does not enter the higher-order calculation of the even eigenvalue below.

At $\mathcal{O}(\varepsilon)$, we obtain

$$\begin{cases} \Phi_{0yy} - (\Phi_0 V_{1y} + U_0\Psi_{1y})_y = 0, & y \in (0,\infty), \\ D\Psi_{1yy} + bh\Phi_0 = 0, & y \in (0,\infty), \\ \Phi_{0y}(0) = \Psi_{1y}(0) = 0, \ \Phi_0(\infty) = 0, \ \Psi_{1y}(\infty) = \text{constant}. \end{cases} \tag{3.24}$$

Note that system (3.24) is the linearization of the leading-order steady-state system (2.7). Differentiating (2.7) with respect to A, with μ fixed, we find that

$$\Phi_0 = \frac{\partial U_0}{\partial A}, \quad \Psi_1 = \frac{\partial V_1}{\partial A}, \quad y \in (0,\infty), \tag{3.25}$$

is a nontrivial even solution of (3.24). This is the same scaling solution used in the Type I stability analysis in [20, Sec. 2.2].

At $\mathcal{O}(\varepsilon^2)$, we obtain

$$\begin{cases} \Phi_{1yy} - (\Phi_1 V_{1y} + U_0\Psi_{2y})_y - (U_1\Psi_{1y} + \Phi_0 V_{2y})_y = 0, & y \in (0,\infty), \\ D\Psi_{2yy} + bh\Phi_1 - \Psi_0 - b(U_0\Psi_0 + V_0\Phi_0) = \tau\lambda_e\Psi_0, & y \in (0,\infty), \\ \Phi_{1y}(0) = \Psi_{2y}(0) = 0, \ \Phi_1(\infty) = 0. \end{cases} \tag{3.26}$$

Equation (3.26) determines the next-order functions Φ_1 and Ψ_2. Their explicit forms are not needed to determine λ_e, since the latter is obtained from the solvability condition at the next order.

At $\mathcal{O}(\varepsilon^3)$, the equation for Φ_2 is

$$\begin{aligned} \Phi_{2yy} - (\Phi_2 V_{1y} + U_0\Psi_{3y})_y = \big(U_1\Psi_{2y} + \Phi_1 V_{2y} + U_2\Psi_{1y} + \Phi_0 V_{3y}\big)_y \\ + \lambda_e\Phi_0 - \big((r - mh) - 2aU_0\big)\Phi_0, \end{aligned} \quad y \in (0,\infty) \tag{3.27}$$

Integrating (3.27) over $(0,\infty)$, and using the Neumann conditions at $y = 0$ together with the matching behavior as $y \to \infty$, we obtain

$$\lambda_e \int_0^\infty \Phi_0 \, \mathrm{d}y = \int_0^\infty \big((r - mh) - 2aU_0\big)\Phi_0 \, \mathrm{d}y. \tag{3.28}$$

Using (2.11) and (3.25), we have

$$\int_0^\infty \Phi_0 \,\mathrm{d}y = \frac{\partial}{\partial A}\int_0^\infty U_0 \,\mathrm{d}y = \frac{1}{2}\sqrt{\frac{\mu D}{Abh}}, \quad \frac{\int_0^\infty U_0\Phi_0 \,\mathrm{d}y}{\int_0^\infty \Phi_0 \,\mathrm{d}y} = \frac{\mu A}{2} = \bar{A},$$

which together with (3.28) yields

$$\lambda_e = \frac{\int_0^\infty \big((r-mh) - 2aU_0\big)\Phi_0 \,\mathrm{d}y}{\int_0^\infty \Phi_0 \,\mathrm{d}y} = (r-mh) - 2a\bar{A} = -2(r-mh) < 0, \tag{3.29}$$

where we have used $\bar{A} = \frac{\mu A}{2} = \frac{3(r-mh)}{2a}$ given in (2.21).

As in the Type I calculation in [20, Sec. 2.2], an explicit outer solution for ψ is not required to determine the leading-order even eigenvalue. The leading-order eigenvalue λ_e is determined by the inner solvability condition (3.28).

3.1.3 Exclusion of additional spike-core scales

The purely toxicant modes have already been considered above. We now focus on the spike-core spectrum and verify that the large and bounded eigenvalue balances analyzed above are the only algebraic scales arising from regular matched inner-outer expansions. Throughout this subsection, $\tau \geq 0$ is fixed independently of ε.

Consider a normalized eigenpair $(\lambda_\varepsilon, \phi_\varepsilon, \psi_\varepsilon)$ satisfying

$$\operatorname{Re}\lambda_\varepsilon \geq 0,$$

and suppose that ϕ_ε has a nonzero leading-order component in the spike core.

We first exclude eigenvalues larger than the core scale. If $\varepsilon^2|\lambda_\varepsilon| \to \infty$, the leading balances in (3.4), together with the boundary and matching conditions, give successively $\Psi \equiv 0$, $\Phi \equiv 0$. This contradicts the normalization of the eigenfunction. Hence a spike-core eigenvalue cannot be larger than $\mathcal{O}(\varepsilon^{-2})$.

Suppose next that, along a subsequence, $\varepsilon^2\lambda_\varepsilon \to \lambda_{la} \neq 0$. The leading inner problem is then (3.9). Since $\operatorname{Re}\lambda_\varepsilon \geq 0$, we have $\operatorname{Re}\lambda_{la} \geq 0$, which contradicts Theorem 3.1. Thus the large spike-core branch cannot enter the closed right half-plane.

It remains to exclude an unbounded eigenvalue satisfying

$$|\lambda_\varepsilon| \to \infty, \qquad \varepsilon^2|\lambda_\varepsilon| \to 0.$$

At leading order, the inner eigenfunction must lie in the kernel of (3.24). Integrating the first equation of (3.24) once gives

$$\left(\frac{\Phi_0}{U_0} - \Psi_1\right)_y = 0, \qquad \Phi_0 = U_0(\Psi_1 + c).$$

With

$$z = \sqrt{\frac{\bar{A}bh}{2D}}\, y, \qquad f = \Psi_1 + c,$$

the second equation becomes

$$f_{zz} + 2\operatorname{sech}^2 z\, f = 0.$$

Its two linearly independent solutions are

$$\tanh z, \qquad 1 - z\tanh z.$$

The Neumann condition at $z = 0$ excludes $\tanh z$. Hence the admissible even kernel is one-dimensional and is generated by the scaling mode

$$(\Phi_0, \Psi_1) = \left(\frac{\partial U_0}{\partial A}, \frac{\partial V_1}{\partial A}\right).$$

For this mode,

$$\int_0^\infty \Phi_0 \, \mathrm{d}y = \frac{1}{2}\sqrt{\frac{\mu D}{Abh}} \neq 0.$$

Substitution into (3.2) gives

$$\lambda_\varepsilon = \mathcal{O}(1),$$

contradicting $|\lambda_\varepsilon| \to \infty$. Therefore no additional unbounded spike-core scale occurs between $\mathcal{O}(1)$ and $\mathcal{O}(\varepsilon^{-2})$.

We finally consider bounded eigenvalues. For a bounded spike-core eigenvalue, the leading inner component must belong to the admissible even kernel of (3.24). Since this kernel is generated only by the scaling mode, every nontrivial leading core component is proportional to that mode. The solvability condition (3.28) then gives

$$\lambda_\varepsilon = -2(r - mh) + o(1) < 0.$$

If the scaling coefficient vanishes, then the eigenfunction has no nontrivial leading spike-core component and belongs to the purely toxicant mode considered above.

There is also no algebraically small spike-core eigenvalue satisfying $\lambda_\varepsilon = o(1)$. Indeed, the zero modes of the limiting inner problem are the scaling and translational modes. The scaling mode is shifted to

$$\lambda_e = -2(r - mh) \neq 0,$$

whereas the translational mode is odd and does not satisfy the Neumann condition at the center of the boundary spike. Moreover, the outer problem at $\lambda = 0$ is

$$D\psi_{xx} - \psi = 0, \qquad \psi_x(0) = \psi_x(\ell) = 0,$$

which has only the zero solution. Hence the formal zero-eigenvalue problem is nondegenerate.

We have therefore accounted for the algebraic spike-core eigenvalue scales arising within the present matched inner-outer expansion. The large core problem has no nonzero eigenvalue in the closed right half-plane, while the leading bounded scaling eigenvalue is strictly negative. Together with the purely toxicant modes considered above, this gives the formal linear stability of the boundary spike.

Proposition 3.1. *Assume that $r - mh > 0$ and that $\tau \geq 0$ is fixed independently of ε. Then the boundary-spike steady state (u_s, w_s) constructed in Proposition 1.1 is linearly stable as $\varepsilon \to 0^+$.*

The same leading-order calculation applies to the double-boundary pattern. We give a brief formal stability argument for the double boundary spike. The double-boundary-spike equilibrium is even with respect to $x = 0$, so the linearized problem decomposes into even and odd subspaces. Even perturbations reduce on $(0, \ell)$ to the Neumann boundary-spike problem analyzed above. Odd perturbations reduce to the corresponding Dirichlet-Neumann problem, with a Dirichlet condition at $x = 0$ and a Neumann condition at the spike boundary $x = \ell$. For the purely toxicant modes, the leading order eigenvalue problem for the odd perturbation reduces to

$$\tau\lambda\psi = D\psi_{xx} - \psi, \ x \in (0, \ell), \ \psi(0) = 0, \ \psi'(\ell) = 0.$$

For $\tau > 0$, these eigenvalues are real and strictly negative. When $\tau = 0$, the toxicant equation is elliptic and generates no independent eigenvalues.

For the spike-core modes, since the eigenfunctions are localized near $x = \ell$, the change of the remote boundary condition at $x = 0$ does not alter their leading-order inner problems. Consequently, the large-eigenvalue problem has no nonzero eigenvalue in the closed right half-plane and the two leading scaling eigenvalues satisfy

$$\lambda_e = -2(r - mh) + o(1) < 0.$$

Hence the double-boundary spike is linearly stable at leading order.

3.2 Stability of an interior spike

We now show that the interior spike centered at $x = 0$ is unstable with respect to an odd translational eigenvalue. We start with the linearized eigenvalue problem on the symmetric domain $(-\ell, \ell)$:

$$\begin{cases} \lambda\phi = \phi_{xx} - \varepsilon^{-1}(\phi v_{s,x} + u_s\psi_x)_x + ((r - mh)\phi - 2au_s\phi) + m\varepsilon\,(u_s\psi + v_s\phi)\,, \\ \tau\lambda\psi = D\psi_{xx} - \psi + \frac{bh}{\varepsilon}\phi - b(u_s\psi + v_s\phi), \\ \phi_x(\pm\ell) = \psi_x(\pm\ell) = 0, \end{cases} \tag{3.30}$$

where (u_s, v_s) denotes the single interior spike constructed in (1.5), obtained by even reflection of the half-spike profile in (2.42). In particular,

$$u_s(-x) = u_s(x), \quad v_s(-x) = v_s(x), \quad x \in (-\ell, \ell).$$

In the inner region: near the spike center 0, we obtain the eigenvalue problem on the full real line $y \in \mathbb{R}$:

$$\begin{cases} \varepsilon^3\lambda\Phi = \varepsilon\Phi_{yy} - (\Phi V_y + U\Psi_y)_y + \varepsilon^3\left((r - mh) - 2aU\right)\Phi + m\varepsilon^4(U\Psi + V\Phi), \\ \varepsilon^2\tau\lambda\Psi = D\Psi_{yy} + \varepsilon bh\Phi - \varepsilon^2\Psi - b\varepsilon^2(U\Psi + V\Phi), \end{cases} \qquad y \in \mathbb{R}. \tag{3.31}$$

Remark 2. Since the interior spike is symmetric with respect to $x = 0$, the eigenvalue problem (3.30) decomposes into even and odd subspaces. An even eigenfunction on $(-\ell, \ell)$ restricts to the boundary-spike eigenvalue problem on $(0, \ell)$, and conversely an eigenfunction of the boundary-spike problem can be extended evenly to $(-\ell, \ell)$. Hence the even eigenvalues coincide with those studied for the boundary spike. The interior-spike problem additionally admits odd eigenfunctions. In particular, the translational mode belongs to the odd subspace and will be shown below to generate a positive eigenvalue.

We seek the odd eigenvalue and expand

$$\lambda \sim \lambda_o + \mathcal{O}(\varepsilon) + \cdots, \ \Phi \sim \Phi_0 + \varepsilon\Phi_1 + \varepsilon^2\Phi_2 + \cdots, \ \Psi \sim \Psi_0 + \varepsilon\Psi_1 + \varepsilon^2\Psi_2 + \cdots. \tag{3.32}$$

Substituting into (3.31) and collecting terms order by order in ε, we obtain the following hierarchical systems for $y \in \mathbb{R}$.

At order $\mathcal{O}(1)$, we obtain

$$\begin{cases} (\Phi_0 V_{0y} + U_0\Psi_{0y})_y = 0, & y \in \mathbb{R}, \\ D\Psi_{0yy} = 0, & y \in \mathbb{R}. \end{cases} \tag{3.33}$$

Since Ψ_0 is bounded on $\mathbb{R}$, the second equation of (3.33) implies that Ψ_0 is constant. Since Ψ_0 is odd, it follows that

$$\Psi_0 \equiv 0, \quad y \in \mathbb{R}. \tag{3.34}$$

Moreover, $V_0 = C_0$ is constant by (2.6), and hence the first equation of (3.33) is identically satisfied.

At order $\mathcal{O}(\varepsilon)$, we obtain

$$\begin{cases} \Phi_{0yy} - (\Phi_0 V_{1y} + U_0\Psi_{1y})_y = 0, & y \in \mathbb{R}, \\ D\Psi_{1yy} + bh\Phi_0 = 0, & y \in \mathbb{R}. \end{cases} \tag{3.35}$$

Recall that the inner problem (2.7) was originally formulated on the half-line $y \in (0, \infty)$. For the interior spike, we extend its solution evenly to the whole real line by setting

$$\widetilde{U}_0(y) := U_0(|y|), \quad \widetilde{V}_1(y) := V_1(|y|), \quad y \in \mathbb{R}. \tag{3.36}$$

Since $U_{0y}(0) = V_{1y}(0) = 0$, and U_0 and V_1 are smooth on $[0, \infty)$, we see that $\widetilde{U}_0(y)$ and $\widetilde{V}_1(y)$ are smooth across $y = 0$. Moreover, they satisfy

$$\begin{cases} \widetilde{U}_{0yy} - (\widetilde{U}_0 \widetilde{V}_{1y})_y = 0, & y \in \mathbb{R}, \\ D\widetilde{V}_{1yy} + bh\widetilde{U}_0 = 0, & y \in \mathbb{R}. \end{cases} \tag{3.37}$$

For simplicity, we continue to denote the even extensions $(\widetilde{U}_0, \widetilde{V}_1)$ by (U_0, V_1).

Differentiating the full-line system (3.37) with respect to y, we obtain

$$\begin{cases} U_{0yyy} - (U_{0y}V_{1y} + U_0 V_{1yy})_y = 0, & y \in \mathbb{R}, \\ DV_{1yyy} + bhU_{0y} = 0, & y \in \mathbb{R}. \end{cases} \tag{3.38}$$

Comparing (3.38) with (3.35), we find that

$$\Phi_0(y) = U_{0y}(y), \quad \Psi_1(y) = V_{1y}(y), \quad y \in \mathbb{R}, \tag{3.39}$$

satisfies (3.35). Since U_0 and V_1 are even on $\mathbb{R}$, U_{0y} and V_{1y} are odd and hence $\Phi_0(0) = \Psi_1(0) = 0$. Thus (3.39) is the odd solution of (3.35) generated by the translational invariance of the full-line leading-order inner problem, in the same sense as the odd translational solution in [20, Sec. 2.2].

At order $\mathcal{O}(\varepsilon^2)$, we obtain

$$\begin{cases} \Phi_{1yy} - (\Phi_1 V_{1y} + U_0 \Psi_{2y})_y = (U_1 \Psi_{1y} + \Phi_0 V_{2y})_y, & y \in \mathbb{R}, \\ D\Psi_{2yy} + bh\Phi_1 = bV_0\Phi_0, & y \in \mathbb{R}. \end{cases} \tag{3.40}$$

Define the linear operator associated with the leading-order inner problem (2.7) by

$$\mathcal{L} = \begin{pmatrix} \dfrac{\partial^2}{\partial y^2} - V_{1y}\dfrac{\partial}{\partial y} - V_{1yy} & -U_{0y}\dfrac{\partial}{\partial y} - U_0\dfrac{\partial^2}{\partial y^2} \\ bh & D\dfrac{\partial^2}{\partial y^2} \end{pmatrix}. \tag{3.41}$$

Using (3.39), system (3.40) can be written as

$$\mathcal{L}\begin{pmatrix} \Phi_1 \\ \Psi_2 \end{pmatrix} = \begin{pmatrix} (U_1 V_{1yy} + U_{0y} V_{2y})_y \\ bV_0 U_{0y} \end{pmatrix}, \quad y \in \mathbb{R}. \tag{3.42}$$

Differentiating (2.13) with respect to y, we obtain

$$\mathcal{L}\begin{pmatrix} U_{1y} \\ V_{2y} \end{pmatrix} = \begin{pmatrix} (U_1 V_{1yy} + U_{0y} V_{2y})_y \\ bV_0 U_{0y} \end{pmatrix}, \quad y \in \mathbb{R}. \tag{3.43}$$

Subtracting (3.43) from (3.42), we obtain

$$\mathcal{L}\begin{pmatrix} \Phi_1 - U_{1y} \\ \Psi_2 - V_{2y} \end{pmatrix} = \begin{pmatrix} 0 \\ 0 \end{pmatrix}, \quad y \in \mathbb{R}. \tag{3.44}$$

To derive the solvability condition for this system, we consider the adjoint $\mathcal{L}^*$ of $\mathcal{L}$ defined by

$$\mathcal{L}^* = \begin{pmatrix} \dfrac{\partial^2}{\partial y^2} + V_{1y}\dfrac{\partial}{\partial y} & bh \\ -U_{0y}\dfrac{\partial}{\partial y} - U_0\dfrac{\partial^2}{\partial y^2} & D\dfrac{\partial^2}{\partial y^2} \end{pmatrix}. \tag{3.45}$$

We consider the adjoint homogeneous problem

$$\mathcal{L}^*\begin{pmatrix} P \\ Q \end{pmatrix} = \begin{pmatrix} 0 \\ 0 \end{pmatrix}, \quad y \in \mathbb{R}. \tag{3.46}$$

A direct calculation shows that (3.46) admits the odd solution

$$P_o(y) = -bhy, \quad Q_o(y) = V_{1y}(y), \quad y \in \mathbb{R}. \tag{3.47}$$

For convenience, set $F := \Phi_1 - U_{1y}, H := \Psi_2 - V_{2y}$. Then (3.44) can be written as

$$\mathcal{L}\begin{pmatrix} F \\ H \end{pmatrix} = \begin{pmatrix} 0 \\ 0 \end{pmatrix}, \quad y \in \mathbb{R}. \tag{3.48}$$

Multiplying (3.48) by the odd adjoint solution (P_o, Q_o), integrating over $(-R, R)$, and integrating by parts, we obtain

$$0 = \Big[P_o F_y - P_{o,y} F - P_o V_{1y} F - P_o U_0 H_y + P_{o,y} U_0 H + D Q_o H_y - D Q_{o,y} H\Big]_{-R}^{R}. \tag{3.49}$$

Letting $R \to \infty$, and using the exponential decay of U_0 and the matching behavior of the population component, the terms containing F and U_0 vanish. Since $Q_o = V_{1y}, Q_{o,y} = V_{1yy}$, we obtain the solvability condition

$$[(\Psi_2 - V_{2y})_y V_{1y} - (\Psi_2 - V_{2y}) V_{1yy}]_{-\infty}^{+\infty} = 0. \tag{3.50}$$

We next simplify (3.50). Since the steady-state profiles are even and the eigenfunction under consideration is odd, $\Psi_2 - V_{2y}$ is odd and $(\Psi_2 - V_{2y})_y$ is even. Moreover, by (2.12), (2.18), and (2.39),

$$V_{1y}(\pm\infty) = \mp\frac{s_0}{2}, \quad V_{1yy}(\pm\infty) = 0, \quad V_{2yy}(\pm\infty) = \frac{C_0}{D}. \tag{3.51}$$

Substituting (3.51) into (3.50), we obtain $(\Psi_2 - V_{2y})_y(\pm\infty) = 0$. Therefore,

$$\Psi_{2y}(\pm\infty) = V_{2yy}(\pm\infty) = \frac{C_0}{D}. \tag{3.52}$$

In the outer region: away from the spike center, the eigenfunction component ϕ is exponentially small to leading order. Hence the second equation of (3.30) reduces to

$$D\psi_{xx} - (1 + \tau\lambda_o)\psi \sim 0, \quad x \in (-\ell, 0) \cup (0, \ell). \tag{3.53}$$

Recall that $\Psi_0 \equiv 0, \Psi_1 = V_{1y}, V_{1y}(+\infty) = -\frac{s_0}{2}$ and $V_{1y}(-\infty) = \frac{s_0}{2}$. Then matching the inner expansion

$$\Psi \sim \varepsilon\Psi_1 + \varepsilon^2\Psi_2 + \cdots, \quad y \in \mathbb{R},$$

with the outer solution gives

$$\psi(0^+) \sim -\frac{\varepsilon s_0}{2}, \quad \psi(0^-) \sim \frac{\varepsilon s_0}{2}. \tag{3.54}$$

Here (3.54) represents the limiting values of the outer approximation as $x \to 0^{\pm}$. The exact odd eigenfunction itself satisfies $\psi(0) = 0$.

Solving (3.53) subject to (3.54) and $\psi_x(\pm\ell) = 0$, we obtain

$$\psi(x) \sim -\frac{\varepsilon s_0}{2\cosh\left(\ell\sqrt{\frac{1+\tau\lambda_o}{D}}\right)} \begin{cases} \cosh\left(\sqrt{\frac{1+\tau\lambda_o}{D}}(\ell - x)\right), & 0 < x < \ell, \\ -\cosh\left(\sqrt{\frac{1+\tau\lambda_o}{D}}(\ell + x)\right), & -\ell < x < 0. \end{cases} \tag{3.55}$$

Moreover,

$$\psi_x(0^{\pm}) \sim \frac{\varepsilon s_0}{2}\sqrt{\frac{1+\tau\lambda_o}{D}}\tanh\left(\sqrt{\frac{1+\tau\lambda_o}{D}}\ell\right). \tag{3.56}$$

Matching: In the inner variables,

$$\psi_x(\varepsilon y) = \frac{1}{\varepsilon}\Psi_y(y) \sim \Psi_{1y}(y) + \varepsilon\Psi_{2y}(y) + \cdots, \qquad y \in \mathbb{R}. \tag{3.57}$$

Since

$$\Psi_{1y}(\pm\infty) = V_{1yy}(\pm\infty) = 0,$$

matching the $\mathcal{O}(\varepsilon)$ terms in (3.56) and (3.57) yields

$$\Psi_{2y}(\pm\infty) = \frac{s_0}{2}\sqrt{\frac{1+\tau\lambda_o}{D}}\tanh\left(\ell\sqrt{\frac{1+\tau\lambda_o}{D}}\right). \tag{3.58}$$

Combining (3.52) and (3.58), we obtain

$$\frac{s_0}{2}\sqrt{\frac{1+\tau\lambda_o}{D}}\tanh\left(\ell\sqrt{\frac{1+\tau\lambda_o}{D}}\right) - \frac{C_0}{D} = 0. \tag{3.59}$$

By (2.39),

$$C_0 = \frac{s_0\sqrt{D}}{2}\coth\left(\frac{\ell}{\sqrt{D}}\right). \tag{3.60}$$

Substituting (3.60) into (3.59), we obtain

$$\ell\sqrt{\frac{1+\tau\lambda_o}{D}}\tanh\left(\ell\sqrt{\frac{1+\tau\lambda_o}{D}}\right) - \frac{\ell}{\sqrt{D}}\coth\left(\frac{\ell}{\sqrt{D}}\right) = 0. \tag{3.61}$$

We now show that equation (3.61) has a unique positive solution $\lambda_o > 0$ for every $\tau > 0$. Define the function

$$f(z) = z\tanh z - \frac{\ell}{\sqrt{D}}\coth\left(\frac{\ell}{\sqrt{D}}\right).$$

Then equation (3.61) is equivalent to $f\left(\ell\sqrt{\frac{1+\tau\lambda_o}{D}}\right) = 0$.

Note that (i) $f(z)$ is strictly increasing for $z > 0$, (ii) $f(\frac{\ell}{\sqrt{D}}) = \frac{\ell}{\sqrt{D}}\left(\tanh\left(\frac{\ell}{\sqrt{D}}\right) - \coth\left(\frac{\ell}{\sqrt{D}}\right)\right) < 0$, (iii) $\lim_{z\to\infty} f(z) = \infty$. By the intermediate value theorem, there exists a unique $z^* > \frac{\ell}{\sqrt{D}}$ such that $f(z^*) = 0$, which together with (3.61) yields

$$z^* = \ell\sqrt{\frac{1+\tau\lambda_o}{D}}.$$

Hence,

$$\lambda_o = \frac{1}{\tau}\left(\frac{Dz^{*2}}{\ell^2} - 1\right) > 0, \tag{3.62}$$

which means the interior spike is unstable with respect to the odd translational eigenvalue.

Remark 3. When $\tau = \tau_0\varepsilon$ with fixed $\tau_0 \geq 0$, we set $\lambda_o = \varepsilon^{-1}\widehat{\lambda} + \mathcal{O}(1)$. Repeating the inner–outer matching calculation gives

$$\ell\sqrt{\frac{1+\tau_0\widehat{\lambda}}{D}}\tanh\left(\ell\sqrt{\frac{1+\tau_0\widehat{\lambda}}{D}}\right) - \frac{\ell}{\sqrt{D}}\coth\left(\frac{\ell}{\sqrt{D}}\right) + \ell\sqrt{\frac{D}{2bh\bar{A}}}\,\widehat{\lambda} = 0. \tag{3.63}$$

Let $F(\widehat{\lambda})$ denote the left-hand side of (3.63). For $\widehat{\lambda} \geq 0$, F is strictly increasing,

$$F(0) = \frac{\ell}{\sqrt{D}}\left[\tanh\left(\frac{\ell}{\sqrt{D}}\right) - \coth\left(\frac{\ell}{\sqrt{D}}\right)\right] < 0, \qquad F(\widehat{\lambda}) \to +\infty \quad \text{as } \widehat{\lambda} \to +\infty.$$

Thus, (3.63) has a unique positive root $\widehat{\lambda}_*(\tau_0)$, showing that the translational instability persists when $\tau = \mathcal{O}(\varepsilon)$. Moreover, as $\tau_0 \to 0$,

$$\widehat{\lambda}_*(0) = \frac{\sqrt{2bh\bar{A}}}{D}\left[\coth\left(\frac{\ell}{\sqrt{D}}\right) - \tanh\left(\frac{\ell}{\sqrt{D}}\right)\right] > 0,$$

which agrees with the result for the instantaneous-response limit $\tau = 0$.

We summarize our results in the following proposition.

Proposition 3.2. *Assume that $r - mh > 0$ and let $\tau > 0$ be fixed. For the single interior spike centered at $x = 0$, constructed in (1.5) with $n = 1$, the leading-order odd eigenvalue equation (3.61) has a unique positive solution λ_o, and hence the interior spike is linearly unstable as $\varepsilon \to 0^+$.*

Remark 4. The same procedure can be extended to interior multi-spike patterns. In that case, the K local translational modes are coupled through the outer toxicant field, and their leading eigenvalues are determined by a $K \times K$ interaction matrix. A detailed analysis of this matrix is beyond the scope of the present paper.

4 Dynamics of an interior spike

In this section, we analyze the drift dynamics of an interior spike when $\tau = 0$. This corresponds to the case where the toxicant w evolves on a much faster time scale than the population u so that its dynamics are effectively slaved to the spike motion. As established in the previous section, the eigenvalue associated with the translational instability is of order $\mathcal{O}(\varepsilon^{-1})$ when $\tau = 0$. This implies that the spike moves on the fast time scale $T = \varepsilon^{-1}t$ in the homogeneous case. We therefore seek an asymptotic solution of the form $u(x,t) \sim U\left(\frac{x-x_0(T)}{\varepsilon}, t\right)$, where $x_0(T)$ denotes the time-dependent position of the spike center.

4.1 Dynamics of a spike with a weakly heterogeneous input of toxicant

We first analyze the drift dynamics of an interior spike with a weakly heterogeneous toxicant input, namely $h = h_0 + \varepsilon h_1(x)$. The system we consider is

$$\begin{cases} u_t = u_{xx} + \varepsilon^{-2}(uw_x)_x + u(r - mw) - au^2, & x \in (-\ell, \ell), t > 0, \\ 0 = Dw_{xx} + h_0 + \varepsilon h_1(x) - w - buw, & x \in (-\ell, \ell), t > 0, \\ u_x(\pm\ell, t) = 0, \quad w_x(\pm\ell, t) = 0, & t > 0. \end{cases} \tag{4.1}$$

Set $w(x,t) = h_0 - \varepsilon v(x,t)$. Substituting it into (4.1) yields

$$\begin{cases} u_t = u_{xx} - \varepsilon^{-1}(uv_x)_x + u(r - mh_0 + \varepsilon mv) - au^2, & x \in (-\ell, \ell), t > 0, \\ 0 = Dv_{xx} - v - h_1(x) + \varepsilon^{-1}bh_0u - buv, & x \in (-\ell, \ell), t > 0, \\ u_x(\pm\ell, t) = 0, \quad v_x(\pm\ell, t) = 0, & t > 0. \end{cases} \tag{4.2}$$

As established in the previous section, the spike moves on the fast time scale $T = \varepsilon^{-1}t$ when $\tau = 0$. We therefore seek an asymptotic moving spike solution of the form

$$u(x,t) \sim U\left(\frac{x - x_0(T)}{\varepsilon}, t\right),$$

where $x_0(T)$ denotes the time-dependent position of the spike center.

Substituting this ansatz into the original system (4.2) yields:

$$\begin{cases} -\varepsilon^{-1}\frac{\mathrm{d}x_0}{\mathrm{d}T}u_x + \frac{\partial u}{\partial t} = u_{xx} - \varepsilon^{-1}(uv_x)_x + u(r - mh_0 + \varepsilon mv) - au^2, & x \in (-\ell,\ell), t > 0, \\ 0 = Dv_{xx} - v - h_1(x) + \frac{bh_0}{\varepsilon}u - buv, & x \in (-\ell,\ell), t > 0, \\ u_x(\pm\ell, t) = 0, \quad v_x(\pm\ell, t) = 0, & t > 0. \end{cases} \tag{4.3}$$

In the inner region: Near the spike center, let $y = \frac{x - x_0(T)}{\varepsilon}$, and define the inner solutions $U(y,t) = u(x,t)$ and $V(y,t) = v(x,t)$. Substituting into (4.3) transforms the system to the full real line $y \in \mathbb{R}$:

$$\begin{cases} -U_y\frac{\mathrm{d}x_0}{\mathrm{d}T} + \varepsilon^2 U_t = U_{yy} - \varepsilon^{-1}(UV_y)_y + \varepsilon^2(U(r - mh_0 + \varepsilon mV) - aU^2), \\ 0 = DV_{yy} + \varepsilon bh_0 U - \varepsilon^2\left(V + h_1(x_0(T) + \varepsilon y) + bUV\right). \end{cases} \tag{4.4}$$

We look for asymptotic expansions

$$U \sim U_0 + \varepsilon U_1 + \varepsilon^2 U_2 + \cdots, \quad V \sim V_0 + \varepsilon V_1 + \varepsilon^2 V_2 + \cdots, \quad y \in \mathbb{R}, T > 0, \tag{4.5}$$

and solve for $U_j,\ V_j$ at each order of ε.

At the leading order, we obtain

$$\begin{cases} (U_0 V_{0y})_y = 0, & y \in \mathbb{R}, T > 0, \\ DV_{0yy} = 0, & y \in \mathbb{R}, T > 0. \end{cases} \tag{4.6}$$

The only bounded solution as $y \to \pm\infty$ is $V_0 = C_0(t)$, where $C_0(t)$ will be determined by matching with the outer solution.

At the next order, we obtain

$$\begin{cases} U_{0yy} - (U_0 V_{1y})_y = -U_{0y}\frac{\mathrm{d}x_0}{\mathrm{d}T}, & y \in \mathbb{R}, T > 0, \\ DV_{1yy} + bh_0 U_0 = 0, & y \in \mathbb{R}, T > 0. \end{cases} \tag{4.7}$$

Solving the first equation with $U_{0y}(0) = U_{0y}(\infty) = 0$, we obtain

$$U_0(y,t) = \bar{A}(t)e^{V_1(y) - V_1(0) - \frac{\mathrm{d}x_0}{\mathrm{d}T}y}, \tag{4.8}$$

where $\bar{A}(t)$ will be determined below. Plugging (4.8) into the second equation yields

$$DV_{1yy} + bh_0\bar{A}(t)e^{V_1 - V_1(0) - \frac{\mathrm{d}x_0}{\mathrm{d}T}y} = 0. \tag{4.9}$$

Substituting (4.8) into the second equation of (4.7) and defining

$$\overline{V}_1(y,t) = V_1(y) - V_1(0) - \frac{dx_0}{dT}y,$$

we obtain

$$D\overline{V}_{1yy} + bh_0\bar{A}(t)e^{\overline{V}_1} = 0,$$

with boundary conditions $\overline{V}_1(0,t) = 0$ and $\overline{V}_{1y}(0,t) = 0$. The unique solution is

$$\overline{V}_1(y,t) = \ln\left(\operatorname{sech}^2\left(\sqrt{\frac{bh_0\bar{A}(t)}{2D}}y\right)\right).$$

Therefore,

$$U_0 = \bar{A}(t)\operatorname{sech}^2(y\sqrt{\frac{\bar{A}(t)bh_0}{2D}}). \tag{4.10}$$

A direct calculation gives the following integrals:

$$\int_{-\infty}^{\infty} U_0 \,\mathrm{d}y = 2\sqrt{\frac{2D\bar{A}}{bh_0}}, \quad \int_{-\infty}^{\infty} U_0^2 \,\mathrm{d}y = \frac{4}{3}\sqrt{\frac{2D}{bh_0}}\,\bar{A}^{3/2}. \tag{4.11}$$

Integrating the first equation of (4.4) over $\mathbb{R}$, and using the decay of U and UV_y as $y \to \pm\infty$, we obtain

$$\frac{\partial \int_{-\infty}^{\infty} U_0 \,\mathrm{d}y}{\partial t} = (r - mh_0)\int_{-\infty}^{\infty} U_0 \,\mathrm{d}y \; - a\int_{-\infty}^{\infty} U_0^2 \,\mathrm{d}y,$$

which reduces to

$$\frac{d\bar{A}}{\mathrm{d}t} = 2(r - mh_0)\bar{A} - \frac{4a}{3}\bar{A}^2.$$

Then the far-field behavior of V_1 is

$$V_1(y,t) \sim \left(\mp\sqrt{\frac{2bh_0\bar{A}(t)}{D}} + \frac{dx_0}{dT}\right) y + V_1(0) + 2\ln 2, \quad V_{1y}(y,t) \to \mp\sqrt{\frac{2bh_0\bar{A}(t)}{D}} + \frac{dx_0}{dT}, \quad y \to \pm\infty. \tag{4.12}$$

In the outer region: Away from the spike center, u is exponentially small and v satisfies

$$Dv_{xx} - v - h_1(x) = -Ds_0(t)\delta(x - x_0(T)), \quad v_x(\pm\ell, t) = 0, \tag{4.13}$$

where $s_0(t)$ is the strength of the delta-function source induced by the inner solution. The solution is

$$v = s_0(t)G(x, x_0) + \bar{v}, \tag{4.14}$$

where $\bar{v}$ is the solution to

$$D\bar{v}_{xx} - \bar{v} - h_1(x) = 0, \;\; \bar{v}_x(\pm\ell) = 0, \tag{4.15}$$

s_0 will be determined below and $G(x, x_0)$ is the Green's function satisfying

$$DG_{xx} - G = -D\delta(x - x_0), \;\; G_x(\pm\ell) = 0. \tag{4.16}$$

We solve (4.16) to obtain

$$G(x, x_0) = \frac{\sqrt{D}}{(\tanh\frac{\ell - x_0}{\sqrt{D}} + \tanh\frac{\ell + x_0}{\sqrt{D}})} \cdot \begin{cases} \frac{1}{\cosh\left((\ell - x_0)/\sqrt{D}\right)}\cosh\left(\frac{\ell - x}{\sqrt{D}}\right), & x_0 < x < \ell, \\ \frac{1}{\cosh\left((\ell + x_0)/\sqrt{D}\right)}\cosh\left(\frac{\ell + x}{\sqrt{D}}\right), & -\ell < x < x_0. \end{cases} \tag{4.17}$$

Matching the far-field behavior of the inner solution with the outer solution, we obtain

$$\begin{aligned} s_0(t)G(x_0, x_0) + \bar{v}(x_0) &= C_0(t), \\ s_0(t)\left(G_x(x_0^+, x_0) - G_x(x_0^-, x_0)\right) &= -2\sqrt{\frac{2bh_0\bar{A}(t)}{D}}, \\ 2\bar{v}_x(x_0) + s_0(t)\left(G_x(x_0^+, x_0) + G_x(x_0^-, x_0)\right) &= 2\frac{\mathrm{d}x_0}{\mathrm{d}T}. \end{aligned} \tag{4.18}$$

Solving these equations yields

$$s_0(t) = 2\sqrt{\frac{2bh_0\bar{A}(t)}{D}}, \tag{4.19}$$

and

$$\begin{aligned} \frac{\mathrm{d}x_0}{\mathrm{d}T} &= \bar{v}_x(x_0) + \frac{s_0\left(G_x(x_0^+, x_0) + G_x(x_0^-, x_0)\right)}{2} \\ &= \bar{v}_x(x_0) + \frac{\sqrt{2bh_0\bar{A}(t)}\left(\tanh\frac{x_0 - \ell}{\sqrt{D}} + \tanh\frac{\ell + x_0}{\sqrt{D}}\right)}{\sqrt{D}(\tanh\frac{\ell - x_0}{\sqrt{D}} + \tanh\frac{\ell + x_0}{\sqrt{D}})}. \end{aligned} \tag{4.20}$$

Returning to the original time scale t, we obtain the reduced system of ODEs governing the spike dynamics:

$$\begin{aligned}\frac{\mathrm{d}x_0}{\mathrm{d}t} &= \frac{1}{\varepsilon}\left(\bar{v}_x(x_0) + \frac{\sqrt{2bh_0\bar{A}(t)}\left(\tanh\frac{x_0-\ell}{\sqrt{D}} + \tanh\frac{\ell+x_0}{\sqrt{D}}\right)}{\sqrt{D}(\tanh\frac{\ell-x_0}{\sqrt{D}} + \tanh\frac{\ell+x_0}{\sqrt{D}})}\right),\\ \frac{\mathrm{d}\bar{A}}{\mathrm{d}t} &= 2(r-mh_0)\bar{A} - \frac{4a}{3}\bar{A}^2.\end{aligned} \tag{4.21}$$

Since the amplitude $\bar{A}$ evolves on a much slower time scale than the position x_0, the drift dynamics can be further approximated by

$$\frac{\mathrm{d}x_0}{\mathrm{d}t} = \frac{1}{\varepsilon}\bar{v}_x(x_0) + \frac{\sqrt{2bh_0\bar{A}_0}\left(\tanh\frac{x_0-\ell}{\sqrt{D}} + \tanh\frac{\ell+x_0}{\sqrt{D}}\right)}{\varepsilon\sqrt{D}(\tanh\frac{\ell-x_0}{\sqrt{D}} + \tanh\frac{\ell+x_0}{\sqrt{D}})}, \tag{4.22}$$

where $\bar{A}_0 = \bar{A}(0)$ is determined by the initial profile.

Remark 5. The steady states of system (4.21) at $h_1 = 0$ correspond to stationary spike patterns in the original PDE. Linearizing (4.21) around the equilibrium $(x_0, \bar{A}) = \left(0, \frac{3(r-mh_0)}{2a}\right)$ recovers the scaling and translational eigenvalues computed in Section 3.

Remark 6. If the population reaction term $u(r-mw) - au^2$ is absent, then the dynamics of x_0 will only be determined by the initial mass. For an initial condition with large mass, that is, when $\bar{A}_0$ is large, the center will move to the boundary.

The validity of (4.21) is demonstrated in Figure 4 for two distinct cases:

- *Homogeneous toxicant input*: $h = h_0$ (constant input rate).
- *Weakly inhomogeneous toxicant input*: $h = h_0 + \varepsilon h_1(x)$. For the numerical example with $\ell = 1,\ D = 1$, we prescribe $\bar{v}_x = -10(1-x^2)(x-0.5), x \in (-1,1)$ so that $\bar{v}_x(x) = 0$ at $x = 0.5$ and set $h_1 = D\bar{v}_{xx} - \bar{v}$.

Full PDE simulations are performed using FlexPDE7 [29]. Since the spike center $x_0(t)$ and amplitude $\bar{A}(t)$ evolve on distinct time scales, we verify their dynamics separately. The initial conditions are chosen as

$$u(x,0) = U_0\left(\frac{x-x_0}{\varepsilon}\right), \quad w(x,0) = h_0,$$

where U_0 is given by (4.10).

The spike center evolves with an $\mathcal{O}(\varepsilon^{-1})$ rate and therefore undergoes an $\mathcal{O}(1)$ displacement on the fast time scale $t = \mathcal{O}(\varepsilon)$. On this time scale,

$$\bar{A}(t) = \bar{A}_0 + \mathcal{O}(\varepsilon), \qquad \bar{A}_0 := \bar{A}(0),$$

so the amplitude remains approximately constant to leading order. We test multiple initial amplitudes $\bar{A}_0$, and all cases yield excellent agreement with our theoretical predictions: for the homogeneous input case ($h = h_0$), the spike drifts toward the domain boundary. For the weakly inhomogeneous case ($h = h_0 + \varepsilon h_1(x)$), the spike moves to the equilibrium of (4.22).

Both drift processes occur over a $\mathcal{O}(\varepsilon)$ time scale. Notably, the equilibrium of (4.22) does not coincide with that of the full system (4.21). When these equilibria differ, the dynamics decouple into three stages : (1) The spike center first migrates to the equilibrium of (4.22) on the $\mathcal{O}(\varepsilon)$ time scale, while the amplitude remains nearly constant; (2) On the slow time scale $t = \mathcal{O}(1)$, the amplitude $\bar{A}(t)$ evolves according to the second equation of (4.21), while the spike center remains close to a stable equilibrium of the first equation corresponding to the current value of

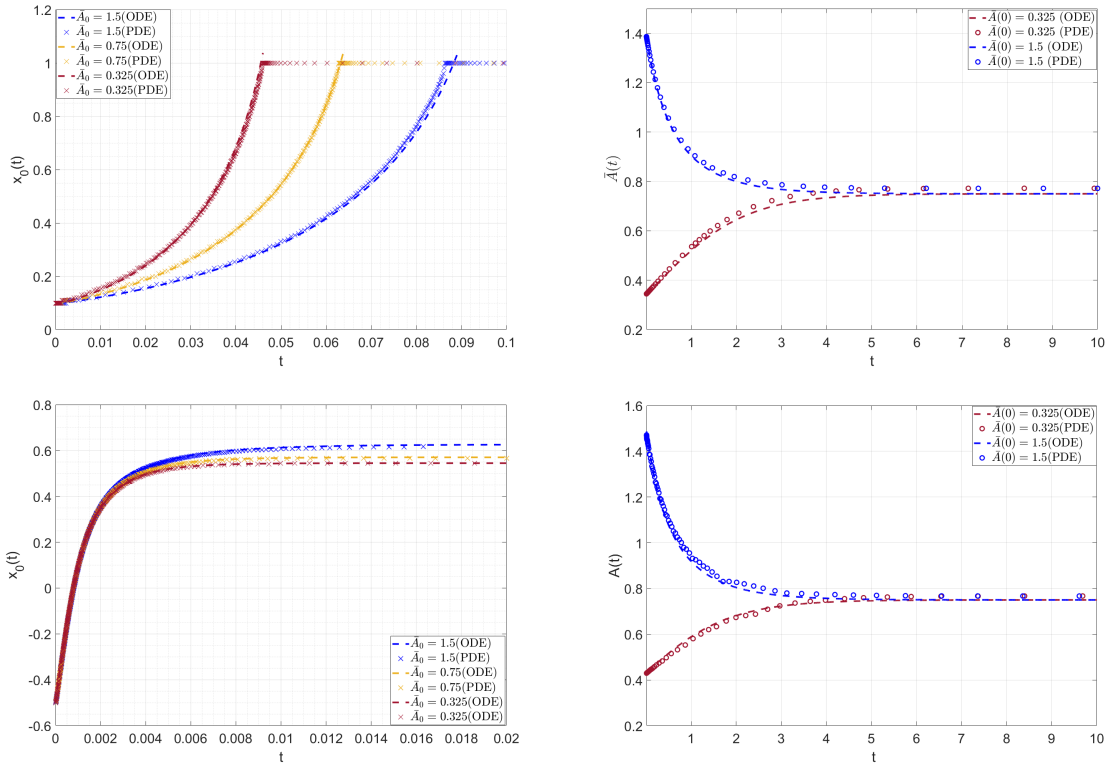


Figure 4: Comparison between the full PDE simulations and the reduced ODE system (4.21). The left column shows the evolution of the spike center, while the right column shows the evolution of the spike height. The top row corresponds to the homogeneous toxicant input, and the bottom row to the weakly heterogeneous input. The PDE results (crosses or circles) are compared with the solutions of the reduced ODE system (dashed curves) for various initial conditions. Parameters are $\varepsilon = 2 \times 10^{-2}, D = 1,\ a = 1, b = 1, m = 0.5,\ r = 1, \tau = \varepsilon^2, \ell = 1$. All the PDE simulations are computed using FlexPDE7 [29].

$\bar{A}(t)$; (3) Once the amplitude crosses a critical threshold, the center resumes moving—this time toward the equilibrium of the full system (4.21)—again on the fast $\mathcal{O}(\varepsilon)$ time scale.

To verify the reduced ODE for $\bar{A}(t)$, we fix the spike center x_0 at its equilibrium position and test various initial amplitudes $\bar{A}(0)$. The numerical results, see the right panel of Figure 4, are in reasonable agreement with the theoretical predictions. Importantly, the leading-order dynamics of $\bar{A}(t)$ are independent of the spatial inhomogeneity of the toxicant input.

4.2 Spike dynamics under strong spatial heterogeneity in the toxicant input

We now consider system (4.23) when $h = h(x)$ is independent of ε. In this case, the leading-order inner function may depend on the position x_0. We therefore write

$$u(x,t) \sim U\left(\frac{x - x_0(T)}{\varepsilon}, x_0(T), t\right).$$

The system under consideration is

$$\begin{cases} u_t = u_{xx} + \varepsilon^{-2}(uw_x)_x + u(r - mw) - au^2, & x \in (-\ell, \ell), t > 0, \\ 0 = Dw_{xx} + h(x) - w - buw, & x \in (-\ell, \ell), t > 0, \\ u_x(\pm\ell, t) = w_x(\pm\ell, t) = 0, & t > 0. \end{cases} \tag{4.23}$$

Set $w = \bar{w}(x) - \varepsilon v$, where $\bar{w}(x)$ satisfies

$$D\bar{w}_{xx} + h(x) - \bar{w} = 0, \quad x \in (-\ell, \ell); \quad \bar{w}_x(\pm\ell) = 0. \tag{4.24}$$

Then (4.23) becomes

$$\begin{cases} u_t = u_{xx} + \varepsilon^{-2}(u\bar{w}_x)_x - \varepsilon^{-1}(uv_x)_x + u(r - m\bar{w} + \varepsilon mv) - au^2, & x \in (-\ell, \ell), t > 0, \\ 0 = Dv_{xx} - v + \varepsilon^{-1} b\bar{w}u - buv, & x \in (-\ell, \ell), t > 0, \\ u_x(\pm\ell, t) = 0, \quad v_x(\pm\ell, t) = 0, & t > 0. \end{cases} \tag{4.25}$$

The highest-order term in system (4.25) is $O(\varepsilon^{-2})$, which implies that the dominant dynamics occur on the fast time scale $T = \varepsilon^{-2}t$. Suppose the spike is located at $x_0(T)$, then in the inner region $x = x_0(T) + \varepsilon y$, we have the following system

$$\begin{cases} -\varepsilon^{-1}\frac{\mathrm{d}x_0}{\mathrm{d}T}U_y + \frac{\mathrm{d}x_0}{\mathrm{d}T}U_{x_0} + \varepsilon^2\frac{\partial U}{\partial t} = U_{yy} + \varepsilon^{-1}\left(U\bar{w}_x(x_0 + \varepsilon y)\right)_y - \varepsilon^{-1}(UV_y)_y \\ \qquad\qquad + \varepsilon^2\left(U(r - m\bar{w}(x_0 + \varepsilon y) + \varepsilon mV) - aU^2\right), \quad y \in \mathbb{R}, T > 0, \\ 0 = DV_{yy} - \varepsilon^2 V + \varepsilon b\bar{w}(x_0 + \varepsilon y)U - \varepsilon^2 bUV, \qquad y \in \mathbb{R}, T > 0. \end{cases} \tag{4.26}$$

We expand

$$U \sim U_0 + \varepsilon U_1 + \varepsilon^2 U_2 + \cdots, \quad V \sim V_0 + \varepsilon V_1 + \varepsilon^2 V_2 + \cdots, \quad y \in \mathbb{R}, T > 0. \tag{4.27}$$

Substituting (4.27) into (4.26), and collecting terms of order $\mathcal{O}(\varepsilon^{-1})$ in the first equation of (4.26) and order $\mathcal{O}(1)$ in the second equation of (4.26), we obtain

$$\begin{cases} -\dfrac{\mathrm{d}x_0}{\mathrm{d}T}U_{0y} = \bar{w}_x(x_0)U_{0y} - (U_0V_{0y})_y, & y \in \mathbb{R}, T > 0, \\ 0 = DV_{0yy}, & y \in \mathbb{R}, T > 0. \end{cases} \tag{4.28}$$

Since V_0 is bounded as $y \to \pm\infty$, the second equation of (4.28) gives $V_{0y} \equiv 0$ and $V_0 = C_0(x_0, t)$. Since $U_0(y)$ is a nontrivial localized spike solution, its derivative $U_{0y}(y)$ is not identically zero. Therefore, we derive from (4.28) that

$$\frac{\mathrm{d}x_0}{\mathrm{d}T} = -\bar{w}_x(x_0). \tag{4.29}$$

This means the leading-order drift velocity of the spike depends only on the gradient of the background toxicant concentration, and is independent of the detailed shape of the spike profile.

Next, we consider the dynamics of the spike when it reaches the minimum of $\bar{w}(x)$. Suppose that we start with a spike profile located at x_c satisfying $\bar{w}_x(x_c) = 0$ and $\bar{w}_{xx}(x_c) > 0$. By (4.29), we have $\frac{dx_0}{dT}\Big|_{x_0 = x_c} = 0$. Using

$$\bar{w}_x(x_c + \varepsilon y) = \varepsilon\bar{w}_{xx}(x_c)y + \mathcal{O}(\varepsilon^2), \quad y \in \mathbb{R},$$

the terms of order $\mathcal{O}(1)$ in the first equation of (4.26) and order $\mathcal{O}(\varepsilon)$ in the second equation give

$$\begin{cases} U_{0yy} + \bar{w}_{xx}(x_c)(yU_0)_y - (U_0V_{1y})_y = 0, & y \in \mathbb{R}, T > 0, \\ DV_{1yy} + b\bar{w}(x_c)U_0 = 0, & y \in \mathbb{R}, T > 0. \end{cases} \tag{4.30}$$

Integrating the first equation of (4.30) once and using the decay of U_0 as $|y| \to \infty$, we obtain

$$U_{0y} + \bar{w}_{xx}(x_c)yU_0 - U_0V_{1y} = 0, \quad y \in \mathbb{R}, T > 0.$$

Hence

$$\frac{U_{0y}}{U_0} = V_{1y} - \bar{w}_{xx}(x_c)y,$$

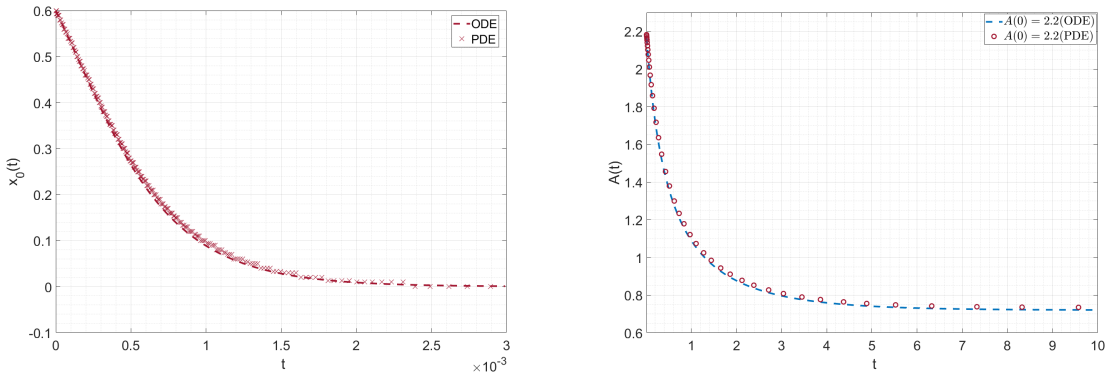


Figure 5: Comparison between the full PDE simulations and the reduced dynamics in the strongly heterogeneous case. The left panel shows the motion of an off-center spike initialized at $x_0(0) = 0.6$; the PDE results are compared with the solution of the center equation (4.29). The minimum of the background toxicant concentration $\bar{w}$ is located at $x_c = 0$. The right panel shows the height evolution of spikes initialized at x_c with several values of $\bar{A}_0$; the PDE results are compared with (4.33). Parameters are $\varepsilon = 2 \times 10^{-2}$, $D = 1$, $a = 1$, $b = 1$, $m = 0.5$, $r = 1$, $\tau = \varepsilon^3$, and $\ell = 1$. All PDE simulations are computed using FlexPDE7 [29].

and therefore

$$U_0(y,T) = \bar{A}(t) \exp\left[V_1(y,T) - V_1(0,T) - \frac{1}{2}\bar{w}_{xx}(x_c)y^2\right], \quad y \in \mathbb{R}, T \geq 0. \tag{4.31}$$

Let $\overline{V}_1 = V_1(y,T) - V_1(0,T) - \frac{1}{2}\bar{w}_{xx}(x_c)y^2$. Then $U_0 = \bar{A}(t)e^{\overline{V}_1}$ and $\overline{V}_1$ is uniquely determined by $\bar{A}(t)$. Substituting this relation into the second equation of (4.30) gives

$$\begin{cases} D\overline{V}_{1yy} + b\bar{w}(x_c)\bar{A}(t)e^{\overline{V}_1} = -D\bar{w}_{xx}(x_c), & y \in \mathbb{R}, T > 0, \\ \overline{V}_1(0,T) = 0, \quad \overline{V}_{1y}(0,T) = 0, & T > 0. \end{cases} \tag{4.32}$$

In general, no explicit solution of (4.32) is available, and the integrals involving U_0 below are evaluated numerically.

Integrating the first equation of (4.26) over $\mathbb{R}$, using $x_0 = x_c$ and the decay of U, and taking the leading order gives the evolution of $\bar{A}(t)$ implicitly

$$\frac{\mathrm{d}\int_{-\infty}^{\infty} U_0 \, dy}{\mathrm{d}t} = (r - m\bar{w}(x_c)) \int_{-\infty}^{\infty} U_0 \, \mathrm{d}y - a\int_{-\infty}^{\infty} U_0^2 \, \mathrm{d}y. \tag{4.33}$$

We verify the validity of (4.29) and (4.33) in Figure 5. We choose the toxicant input as

$$h = 1 + \frac{1}{D\left(\frac{\pi}{\ell}\right)^2 + 1} - \cos\left(\frac{\pi}{\ell}x\right),$$

for which the background toxicant concentration satisfies

$$\bar{w} = 1 + \frac{1}{D\left(\frac{\pi}{\ell}\right)^2 + 1} - \frac{1}{D\left(\frac{\pi}{\ell}\right)^2 + 1}\cos\left(\frac{\pi}{\ell}x\right).$$

To verify the center-motion equation (4.29), we choose an off-center initial spike located at $x_0(0) = x_{0,\mathrm{in}} \neq x_c$:

$$u(x,0) = \bar{A}_0 \exp\left(-\frac{(x - x_{0,\mathrm{in}})^2}{\varepsilon^2}\right), \qquad w(x,0) = \bar{w}(x). \tag{4.34}$$

In the numerical experiment shown in the left panel of Figure 5, we take $x_{0,\mathrm{in}} = 0.6$, whereas the minimum of $\bar{w}$ is located at $x_c = 0$. The numerically computed spike center is compared with the solution of

$$\frac{\mathrm{d}x_0}{\mathrm{d}t} = -\frac{1}{\varepsilon^2}\bar{w}_x(x_0), \qquad x_0(0) = x_{0,\mathrm{in}}.$$

The spike moves toward x_c on the $\mathcal{O}(\varepsilon^2)$ time scale. During this fast translation, its height and profile may also change, but these changes do not affect the leading-order center equation.

To verify the slow height equation (4.33), we perform a separate set of simulations in which the spike is initially centered at the minimum x_c. We prescribe

$$u(x,0) = U_0\left(\frac{x - x_c}{\varepsilon}; \bar{A}_0\right), \qquad w(x,0) = \bar{w}(x), \tag{4.35}$$

where $U_0(\,\cdot\,;\bar{A}_0)$ is determined by (4.31)–(4.32) with initial height $\bar{A}_0$. The spike center then remains at x_c to leading order, while its height evolves according to (4.33). Several values of $\bar{A}_0$ are used in the right panel of Figure 5.

5 Conclusion and discussion

In this paper, we constructed asymptotic localized spike profiles for a toxicant-mediated population model in one spatial dimension in the large toxicant-taxis limit ($\chi \to \infty$ or $\varepsilon \to 0$). We performed a formal spectral analysis showing that the limiting large-core problem has no nonzero eigenvalue in the closed right half-plane, while the leading bounded scaling eigenvalue is strictly negative. The interior spike, in contrast, has a positive translational eigenvalue. In the homogeneous case, this instability drives an off-center interior spike toward the nearest boundary, consistent with the predominance of boundary spikes observed in our numerical simulations.

To characterize the transient dynamics of unstable interior spikes, we derived a reduced system of ordinary differential equations that captures both the fast drift motion of the spike center and the slow evolution of the spike amplitude. This reduced system provides a computationally efficient framework for predicting the long-term behavior of the full partial differential equation system. Direct analysis of the reduced system shows that spikes will drift toward regions of minimal toxicant concentration. Notably, this preferred location does not coincide with the minimum of the external toxicant input, as the local toxicant concentration is self-regulated by the population itself through consumption and degradation processes.

It would be interesting to consider the case when the toxicant input is time dependent, namely $h = h(x,t)$. As a first step, one may directly extend the analysis to the case of a time-dependent toxicant input $h = h(t)$. Since the drift motion of the spike occurs on a fast time scale, the temporal variation of $h(t)$ does not affect the leading-order drift dynamics provided that $h(t)$ varies on an $\mathcal{O}(1)$ time scale. Instead, the influence of time-dependent toxicant input manifests only in the slow evolution of the spike amplitude.

The extension of our results to two and higher spatial dimensions is a major open problem. In two dimensions, the geometry of the domain exerts a profound influence on both the existence and stability of spike solutions. The effect of geometry on localized patterns in 2-D or 3-D has been extensively explored in reaction-diffusion systems [9, 35, 36, 39]. Similarly to patterns observed in the Keller-Segel model, higher-dimensional settings can give rise to more intricate spatial structures, including spots [23], rings [5], stripes [19], and mesa-like configurations [4], which are not observed in one-dimensional settings. It would be interesting to investigate new patterns in two dimensions and determine whether boundary spikes remain stable in non-convex domains, or whether interior spikes can be stabilized near corners or other geometric features.

Acknowledgment. The research of Zhenzhen Li was supported by the National Natural Science Foundation of China (Grant No. 12601328). The research of Zhi-An Wang was supported by a grant from the Research Grants Council of Hong Kong (Project No. PolyU15302825 for

GRF project) and the Hong Kong Scholars Program (Project ID P0048916). The research of Shuangquan Xie was supported by the National Natural Science Foundation of China (Grant NO. 12401198).

A Positivity of a nonlocal quadratic form

Lemma A.1. *Let $p(z) = 2\operatorname{sech}^2 z$ and define*

$$Q[f] := \int_0^\infty |f_z|^2 \,\mathrm{d}z - \int_0^\infty p(z)|f(z)|^2 \,\mathrm{d}z + \frac{1}{\int_0^\infty p(z)\,\mathrm{d}z}\left|\int_0^\infty p(z)f(z)\,\mathrm{d}z\right|^2. \tag{A.1}$$

Then

$$Q[f] \geq 0 \tag{A.2}$$

for every $f \in H^1(0,\infty)$. Moreover, if $f(z) \to 0$ as $z \to +\infty$, then equality in (A.2) *holds if and only if $f \equiv 0$. In particular, every eigenvalue η of the nonlocal eigenvalue problem*

$$\begin{cases} f_{zz} + p(z)\left(f - \frac{\int_0^\infty p(s)f(s)\,\mathrm{d}s}{\int_0^\infty p(s)\,\mathrm{d}s}\right) = \eta f, & z \in (0,\infty), \\ f_z(0) = 0, \quad f(z) \to 0 \quad \text{as } z \to +\infty, \end{cases} \tag{A.3}$$

associated with a nontrivial eigenfunction satisfies $\eta < 0$.

Proof. Set $\varpi = \tanh z$ for $0 \leq \varpi < 1$, and define $F(\varpi) := f(\operatorname{arctanh}\varpi)$. Since

$$\frac{d\varpi}{dz} = \operatorname{sech}^2 z = 1 - \varpi^2,$$

we have $\mathrm{d}z = \frac{\mathrm{d}\varpi}{1-\varpi^2}$ and hence

$$\int_0^\infty |f_z|^2 \,\mathrm{d}z = \int_0^1 (1-\varpi^2)|F_\varpi|^2 \,\mathrm{d}\varpi. \tag{A.4}$$

Moreover, $p(z)\,\mathrm{d}z = 2\operatorname{sech}^2 z\,\mathrm{d}z = 2\,\mathrm{d}\varpi$, so that

$$\int_0^\infty p(z)|f(z)|^2 \,\mathrm{d}z = 2\int_0^1 |F(\varpi)|^2 \,\mathrm{d}\varpi \tag{A.5}$$

and

$$\int_0^\infty p(z)f(z)\,\mathrm{d}z = 2\int_0^1 F(\varpi)\,\mathrm{d}\varpi. \tag{A.6}$$

Define $\overline{F} := \int_0^1 F(\varpi)\,\mathrm{d}\varpi$. Since $\int_0^\infty p(z)\,\mathrm{d}z = 2$, using (A.4)–(A.6), we obtain

$$Q[f] = \int_0^1 (1-\varpi^2)|F_\varpi|^2 \,\mathrm{d}\varpi - 2\int_0^1 |F - \overline{F}|^2 \,\mathrm{d}\varpi. \tag{A.7}$$

We now estimate the right-hand side of (A.7). Extend F evenly to $(-1,1)$ by

$$\widetilde{F}(\varpi) := F(|\varpi|).$$

By the definition of $\overline{F}$, $\frac{1}{2}\int_{-1}^1 \widetilde{F}(\varpi)\,\mathrm{d}\varpi = \overline{F}$. Hence, by setting $g(\varpi) := \widetilde{F}(\varpi) - \overline{F}$, we have $\int_{-1}^1 g(\varpi)\,\mathrm{d}\varpi = 0$.

Consider the Legendre Sturm–Liouville operator $\mathcal{L}\varphi := -\frac{\mathrm{d}}{\mathrm{d}\varpi}\left((1-\varpi^2)\varphi_\varpi\right)$ with domain

$$D(\mathcal{L}) := \left\{ \varphi \in L^2(-1,1) : \begin{array}{c} \varphi \in AC_{\mathrm{loc}}(-1,1), \\ (1-\varpi^2)\varphi_\varpi \in H^1(-1,1), \\ \lim\limits_{\varpi\to\pm1}(1-\varpi^2)\varphi_\varpi(\varpi) = 0 \end{array} \right\}.$$

Here $AC_{\mathrm{loc}}(-1,1)$ denotes the space of functions that are absolutely continuous on every compact subinterval of $(-1,1)$. For $\varphi \in D(\mathcal{L})$, we have $\mathcal{L}\varphi = -\big((1-\varpi^2)\varphi_\varpi\big)_\varpi \in L^2(-1,1)$, where the derivative is understood in the weak sense. Its associated quadratic-form domain is

$$\mathcal{V} := \left\{ \varphi \in L^2(-1,1) : \varphi \in AC_{\mathrm{loc}}(-1,1),\ \sqrt{1-\varpi^2}\,\varphi_\varpi \in L^2(-1,1) \right\}.$$

It is classical that the Legendre polynomials P_n satisfy

$$\mathcal{L}P_n = n(n+1)P_n, \qquad n = 0,1,2,\ldots;$$

see, for example, [27, Sec. 18.8, Table 18.8.1] or [33, Ch. IV]. Thus the eigenvalues of $\mathcal{L}$ are

$$\lambda_n = n(n+1), \qquad n = 0,1,2,\ldots.$$

In particular, $\lambda_0 = 0, P_0 \equiv 1$, and the first nonzero eigenvalue is $\lambda_1 = 2$, which corresponds to the eigenfunction $P_1(\varpi) = \varpi$. Define the zero-mean subspace

$$\mathcal{V}_0 := \left\{ \varphi \in \mathcal{V} : \int_{-1}^{1} \varphi(\varpi)\,\mathrm{d}\varpi = 0 \right\}.$$

Since the eigenspace corresponding to $\lambda_0 = 0$ consists of the constant functions, the fact that $g \in \mathcal{V}_0$ is precisely the orthogonality condition to the null eigenspace in $L^2(-1,1)$. By the Rayleigh–Ritz characterization, we have

$$\lambda_1 = \inf_{\substack{0 \neq g \in \mathcal{V} \\ \int_{-1}^{1} g(\varpi)\,\mathrm{d}\varpi = 0}} \frac{\int_{-1}^{1} (1-\varpi^2)|g_\varpi|^2\,\mathrm{d}\varpi}{\int_{-1}^{1} |g|^2\,\mathrm{d}\varpi} = 2.$$

Hence, for every $g \in \mathcal{V}_0$,

$$\int_{-1}^{1} (1-\varpi^2)|g_\varpi|^2\,\mathrm{d}\varpi \geq 2\int_{-1}^{1} |g|^2\,\mathrm{d}\varpi. \tag{A.8}$$

Using $g_\varpi = \widetilde{F}_\varpi$ and $g = \widetilde{F} - \overline{F}$, we rewrite (A.8) as

$$\int_{-1}^{1} (1-\varpi^2)|\widetilde{F}_\varpi|^2\,\mathrm{d}\varpi \geq 2\int_{-1}^{1} |\widetilde{F} - \overline{F}|^2\,\mathrm{d}\varpi. \tag{A.9}$$

Since $\widetilde{F}$ is even, dividing (A.9) by 2 yields

$$\int_{0}^{1} (1-\varpi^2)|F_\varpi|^2\,\mathrm{d}\varpi \geq 2\int_{0}^{1} |F - \overline{F}|^2\,\mathrm{d}\varpi. \tag{A.10}$$

Combining (A.10) with (A.7), we obtain $Q[f] \geq 0$.

It remains to characterize the equality case. Equality in (A.8) can occur only when g belongs to the eigenspace associated with $\lambda_1 = 2$. Therefore, $g(\varpi) = cP_1(\varpi) = c\varpi$ for some constant c. However, $\widetilde{F}$ is even, and hence $g = \widetilde{F} - \overline{F}$ is also even, whereas $P_1(\varpi) = \varpi$ is odd, which means that $c = 0$, and thus,

$$\widetilde{F} \equiv \overline{F}.$$

Hence F is constant on $(0,1)$, and therefore f is constant on $(0,\infty)$. Since $f \in H^1(0,\infty) \subset L^2(0,\infty)$, the only constant function in this space is the zero function. Thus

$$Q[f] = 0 \quad \Longleftrightarrow \quad f \equiv 0.$$

Finally, let (f,η) be a nontrivial eigenpair of (A.3). Multiplying the first equation of (A.3) by $\overline{f}$, integrating over $(0,\infty)$, and integrating by parts, we obtain

$$\eta \int_0^\infty |f|^2\,\mathrm{d}z = -Q[f].$$

Since $f \not\equiv 0$, the strict equality characterization above gives $Q[f] > 0$. Therefore,

$$\eta = -\frac{Q[f]}{\int_0^\infty |f|^2\,\mathrm{d}z} < 0.$$

This completes the proof. □

References

[1] K. O. Achema and C. J. Alhassan. Effect of biodegradable multiple pesticides on aquatic biospecies. In R. E. Rebolledo Ranz, editor, *Insecticides–Impact and Benefits of Its Use for Humanity*, pages 225–244. IntechOpen, 2022.

[2] G. J. Atchison, M. G. Henry, and M. B. Sandheinrich. Effects of metals on fish behavior: a review. *Environmental Biology of Fishes*, 18(1):11–25, 1987.

[3] J. H. S. Blaxter and C. C. ten Hallers-Tjabbes. The effect of pollutants on sensory systems and behaviour of aquatic animals. *Netherlands Journal of Aquatic Ecology*, 26(1):43–58, 1992.

[4] J. A. Carrillo, X. Chen, Q. Wang, Z. Wang, and L. Zhang. Phase transitions and bump solutions of the Keller–Segel model with volume exclusion. *SIAM Journal on Applied Mathematics*, 80(1):232–261, 2020.

[5] L. Chen, F. Kong, and Q. Wang. Stationary ring and concentric-ring solutions of the Keller–Segel model with quadratic diffusion. *SIAM Journal on Mathematical Analysis*, 52(5):4565–4615, 2020.

[6] L. Chen, F. Kong, and Q. Wang. Global and exponential attractor of the repulsive Keller–Segel model with logarithmic sensitivity. *European Journal of Applied Mathematics*, 32(4):599–617, 2021.

[7] J. Chu. Steady states of a diffusive population-toxicant model with negative toxicant-taxis. *Acta Applicandae Mathematicae*, 190(1):13, 2024.

[8] J. Chu, K.-Y. Lam, and Z.-A. Wang. Global dynamics of a diffusive population-toxicant model with toxicant-taxis in time-periodic environments. *SIAM Journal on Applied Mathematics*, 2026. In press.

[9] S. Deng, J. Tzou, and S. Xie. Oscillatory instabilities of a one-spot pattern in the Schnakenberg reaction-diffusion system in 3-D domains, 2024.

[10] X. Deng, Q. Huang, and Z.-A. Wang. Global dynamics and pattern formation in a diffusive population-toxicant model with negative toxicant-taxis. *SIAM Journal on Applied Mathematics*, 83(6):2212–2236, 2023.

[11] S.-I. Ei, H. Izuhara, and M. Mimura. Spatio-temporal oscillations in the Keller–Segel system with logistic growth. *Physica D: Nonlinear Phenomena*, 277:1–21, 2014.

[12] T. G. Hallam, C. E. Clark, and G. S. Jordan. Effects of toxicants on populations: a qualitative approach ii. first order kinetics. *Journal of Mathematical Biology*, 18(1):25–37, 1983.

[13] T. G. Hallam, C. E. Clark, and R. R. Lassiter. Effects of toxicants on populations: a qualitative approach i. equilibrium environmental exposure. *Ecological Modelling*, 18(3–4):291–304, 1983.

[14] T. G. Hallam and J. T. De Luna. Effects of toxicants on populations: a qualitative approach iii. environmental and food chain pathways. *Journal of Theoretical Biology*, 109(3):411–429, 1984.

[15] Q. Huang, L. Parshotam, H. Wang, C. Bampfylde, and M. A. Lewis. A model for the impact of contaminants on fish population dynamics. *Journal of Theoretical Biology*, 334:71–79, 2013.

[16] Q. Huang, G. Seo, and C. Shan. Bifurcations and global dynamics in a toxin-dependent aquatic population model. *Mathematical Biosciences*, 296:26–35, 2018.

[17] J. Jiang. On a repulsion Keller–Segel system with a logarithmic sensitivity. *European Journal of Applied Mathematics*, 33(1):153–181, 2022.

[18] H.-Y. Jin, K.-Y. Lam, and Z.-A. Wang. Global dynamics of the toxicant-taxis model with Robin boundary conditions. *Calculus of Variations and Partial Differential Equations*, 64(8):270, 2025.

[19] L. Jin, Q. Wang, and Z. Zhang. Pattern formation in Keller–Segel chemotaxis models with logistic growth. *International Journal of Bifurcation and Chaos*, 26(2):1650033, 2016.

[20] T. Kolokolnikov, J. Wei, and A. Alcolado. Basic mechanisms driving complex spike dynamics in a chemotaxis model with logistic growth. *SIAM Journal on Applied Mathematics*, 74(5):1375–1396, 2014.

[21] F. Kong, M. J. Ward, and J. Wei. Existence, stability and slow dynamics of spikes in a 1D minimal Keller–Segel model with logistic growth. *Journal of Nonlinear Science*, 34(3):51, 2024.

[22] F. Kong, J. Wei, and L. Xu. The existence and stability of spikes in the one-dimensional Keller–Segel model with logistic growth. *Journal of Mathematical Biology*, 86(1):6, 2023.

[23] F. Kong, J. Wei, and L. Xu. Existence of multi-spikes in the Keller–Segel model with logistic growth. *Mathematical Models and Methods in Applied Sciences*, 33(11):2227–2270, 2023.

[24] K. Kuto, K. Osaki, T. Sakurai, and T. Tsujikawa. Spatial pattern formation in a chemotaxis-diffusion-growth model. *Physica D: Nonlinear Phenomena*, 241(19):1629–1639, 2012.

[25] G. Lan, C. Wei, and S. Zhang. Long time behaviors of single-species population models with psychological effect and impulsive toxicant in polluted environments. *Physica A: Statistical Mechanics and its Applications*, 521:828–842, 2019.

[26] M. Ma, C. Ou, and Z.-A. Wang. Stationary solutions of a volume-filling chemotaxis model with logistic growth and their stability. *SIAM Journal on Applied Mathematics*, 72(3):740–766, 2012.

[27] F. W. J. Olver, D. W. Lozier, R. F. Boisvert, and C. W. Clark, editors. *NIST Handbook of Mathematical Functions*. Cambridge University Press, New York, 2010.

[28] K. J. Painter and T. Hillen. Spatio-temporal chaos in a chemotaxis model. *Physica D: Nonlinear Phenomena*, 240(4–5):363–375, 2011.

[29] PDE Solutions Inc. FlexPDE 7. `https://www.pdesolutions.com/`, 2020.

[30] K. Peters, M. Bundschuh, and R. B. Schäfer. Review on the effects of toxicants on freshwater ecosystem functions. *Environmental Pollution*, 180:324–329, 2013.

[31] G. R. Scott and K. A. Sloman. The effects of environmental pollutants on complex fish behaviour: integrating behavioural and physiological indicators of toxicity. *Aquatic Toxicology*, 68(4):369–392, 2004.

[32] H. Shen, Y. Song, and Q. Huang. Pattern formation driven by toxicant-taxis and delay in a diffusive population-toxicant model. *Communications in Nonlinear Science and Numerical Simulation*, 152:109440, 2026.

[33] G. Szegő. *Orthogonal Polynomials*, volume 23 of *American Mathematical Society Colloquium Publications*. American Mathematical Society, Providence, RI, 4 edition, 1975.

[34] D. M. Thomas, T. W. Snell, and S. M. Jaffar. A control problem in a polluted environment. *Mathematical Biosciences*, 133(2):139–163, 1996.

[35] J. C. Tzou and S. Xie. Oscillatory translational instabilities of spot patterns in the Schnakenberg system on general 2D domains. *Nonlinearity*, 36(5):2473, 2023.

[36] J. C. Tzou, S. Xie, T. Kolokolnikov, and M. J. Ward. The stability and slow dynamics of localized spot patterns for the 3-D Schnakenberg reaction-diffusion model. *SIAM Journal on Applied Dynamical Systems*, 16(1):294–336, 2017.

[37] Q. Wang, J. Yan, and C. Gai. Qualitative analysis of stationary Keller–Segel chemotaxis models with logistic growth. *Zeitschrift für angewandte Mathematik und Physik*, 67(3):51, 2016.

[38] B. W. Wolfe and C. G. Lowe. Movement patterns, habitat use and site fidelity of the white croaker (Genyonemus lineatus) in the Palos Verdes Superfund Site, Los Angeles, California. *Marine Environmental Research*, 109:69–80, 2015.

[39] S. Xie and T. Kolokolnikov. Moving and jumping spot in a two-dimensional reaction–diffusion model. *Nonlinearity*, 30(4):1536, 2017.

[40] J. Xing, Q. Huang, and H. Nie. Dynamical analysis of a diffusive population-toxicant model with toxicant-taxis in polluted aquatic environments. *Mathematical Biosciences*, 372:109193, 2024.